eLife

Reviewed Preprint
v1 • January 5, 2026
Not revised

Reviewed Preprint
v2 • April 17, 2026
Revised by authors

For correspondence:
shaeri.mukherjee@ucsf.edu

Competing interests: No competing interests declared

Funding: See page 21

Reviewing editor: Luke Wiseman, Scripps Research Institute, United States

Hsp70 is phosphorylated in a conserved response to DNA damage and contributes to cell cycle control

Thomas Moss[1,2], Alexandra Wooldredge[1,2], Koustav Bhakta[1,2], Matthew Cronin[1,2], Jason E Gestwicki[3], Shaeri Mukherjee[1,2,4]

[1]G.W. Hooper foundation, University of California, San Francisco, San Francisco, United States • [2]Department of Microbiology and Immunology, University of California, San Francisco, San Francisco, United States • [3]Department of Pharmaceutical Chemistry and the Institute for Neurodegenerative Diseases, University of California, San Francisco, San Francisco, United States • [4]Biohub, San Francisco, United States

eLife Assessment

This potentially **valuable** manuscript focuses on the phosphorylation of residue T495 as a mechanism to inactivate HSP70 and disrupt cell cycle progression in response to DNA damage. The evidence supporting this model is **solid**, but would be significantly strengthened by additional studies defining the extent of T495 phosphorylation induced by DNA damage, identifying the kinase responsible for phosphorylating T495 of HSP70, and further elucidation of the functional implications of T495 phosphorylation in human cells. This work will be of interest to scientists focused on topics including chaperone biology, proteostasis, cell cycle progression, and DNA damage.

https://doi.org/10.7554/eLife.110044.2.sa4

Abstract

Hsp70s are essential molecular chaperones that are increasingly recognized to be regulated by post-translational modifications. Here, we show that phosphorylation of a conserved threonine (T495), previously shown to be exploited by a *Legionella pneumophila* kinase to inhibit Hsp70, occurs endogenously in human cells in response to DNA damage, particularly when base excision repair is overburdened. This modification is cell cycle dependent, and in yeast, phosphomimetic or phosphonull Hsp70 variants disrupt G1/S progression under normal and DNA-damaging conditions. Biochemically, the phosphomimetic T495E mutation locks Hsp70 in an open-like conformation without blocking substrate engagement. Together, our results reveal a conserved mechanism by which dynamic Hsp70 phosphorylation regulates the G1/S transition, and delays cell cycle progression during DNA damage, highlighting how pathogen-derived insights can uncover fundamental cell biology principles.

Introduction

Hsp70s are highly conserved molecular chaperones with wide-ranging roles in cellular homeostasis. At the core of their function is an ATP-driven conformational cycle: Hsp70s alternate between an open ATP-bound state and a closed ADP-bound state, enabling them to bind and release client proteins in a nucleotide-dependent manner[1]. Through this mechanism, Hsp70s participate in diverse biological processes, including protein homeostasis[1], metabolic regulation[2], the DNA damage response[3], and cell cycle control[4–6]. Beyond their central roles in cell biology Hsp70s have been implicated in the pathology of numerous diseases. For example, Hsp70s can inhibit amyloid-beta aggregation *in vitro* and reduce its accumulation in mouse neurons, suggesting protective roles in neurodegenerative diseases such as Alzheimer's disease[7,8]. Hsp70s

are also overexpressed in various cancers and influence tumor cell survival and proliferation [9]. Thus, understanding how Hsp70 activity is regulated has broad implications for both basic biology and therapeutic development.

Hsp70 function is tightly controlled by co-chaperones and post-translational modifications (PTMs). Cochaperones — namely J proteins and nucleotide exchange factors — catalyze nucleotide hydrolysis and exchange, facilitate and specify client engagement, and determine client fate [1]. In recent years, PTMs have emerged as an important layer of regulation. A computational analysis of the budding yeast Hsp70, Ssa1, identified two conserved 'hotspots' in the nucleotide binding domain (NBD) and substrate binding domain (SBD), that are likely regions of PTM-mediated regulation[10]. Experimental work has validated some of the PTMs at these site. For example, T36 in the NBD of Ssa1 is phosphorylated both in response to nutrient stress and exposure to mating pheromone (α-factor), impairing chaperone activity and leading to cell cycle arrest[4]. In mammalian cells, the endoplasmic reticulum (ER) resident Hsp70, BiP, is AMPylated at T518, locking it in an 'open' conformation and tuning its activity to the unfolded protein burden in the ER[11,12]. Our lab previously showed that the *Legionella pnuemophila* (*L.p.*) kinase LegK4 phosphorylates cytosolic human Hsp70 (Hsc70; HSPA8) at T495 during infection, increasing its association with polysomes and globally reducing protein synthesis[13]. Notably, Hsc70(T495) is structurally analogous to BiP(T518), indicating that both AMPylation and phosphorylation at this site have regulatory consequences. This finding led us to ask whether phosphorylation at T495 occurs outside of *L.p.* infection, and if it serves endogenous regulatory functions. Mining phosphoproteomics datasets revealed that the homologous residue in *S. cerevisiae* Ssa1, T492, is phosphorylated during DNA alkylation damage, and when mitotic exit is prevented[14,15]. However, the functional consequences of this modification have not been studied. In this work, we show that Hsp70 is phosphorylated at T495 (pHsp70) in human cells during base excision repair (BER) of DNA damage. We find that a phosphomimetic mutant T495E allosterically impairs ATP hydrolysis *in vitro* and stabilizes an open-like conformation while still permitting substrate engagement. In yeast, the analogous mutation T492E causes a growth defect, leads to accumulation of cells in G1, and delays cell cycle re-entry after alkylation damage. Likewise, the phosphonull mutation (T492A) in yeast lacking a compensatory Hsp70 homolog also causes a growth defect and cell cycle dysregulation after alkylation damage. Together, these data suggest that the dynamic phosphorylation of Hsp70 at this conserved site acts as a regulatory switch to tune chaperone activity in coordination with DNA repair and cell cycle progression.

Results

Phosphomimetic Hsc70 (T495E) is locked in an open-like conformation

Previous work showed that the *Legionella pneumophila* kinase LegK4 phosphorylates Hsc70 at a conserved threonine (T495) in its substrate binding domain (SBD) (Figure 1a,b)[13]. Investigations into the ATPase activity and refolding capacity of *in* vitro phosphorylated Hsc70 indicated that phosphorylation at T495 reduces its chaperone activity[13]. However, *in vitro* phosphorylation by LegK4 only yields phosphorylation of ~53% of the Hsc70, complicating bulk biochemical analyses[13]. To overcome this limitation, we generated a phosphomimetic mutant Hsc70 (T495E). To determine whether this mutant mimics phosphorylated Hsc70, we assessed the ATPase activity of the purified protein using a malachite green assay. As Hsc70 has a low intrinsic rate of ATPase activity, we titrated in the co-chaperone DnaJA2 to stimulate hydrolysis[13,16]. T495E exhibited significantly reduced J-protein stimulated ATPase activity compared to wild-type Hsc70 (WT) (Figure 1c), consistent with prior observations of the LegK4-phosphorylated protein[13]. To investigate if the reduced ATPase activity is due to impaired nucleotide binding, we performed a fluorescence polarization (FP) assay using fluorescently-labeled ATP-FAM. ATP binding was not diminished in T495E (Figure 1d), suggesting that T495E allosterically inhibits J protein stimulated ATPase activity without preventing nucleotide binding.

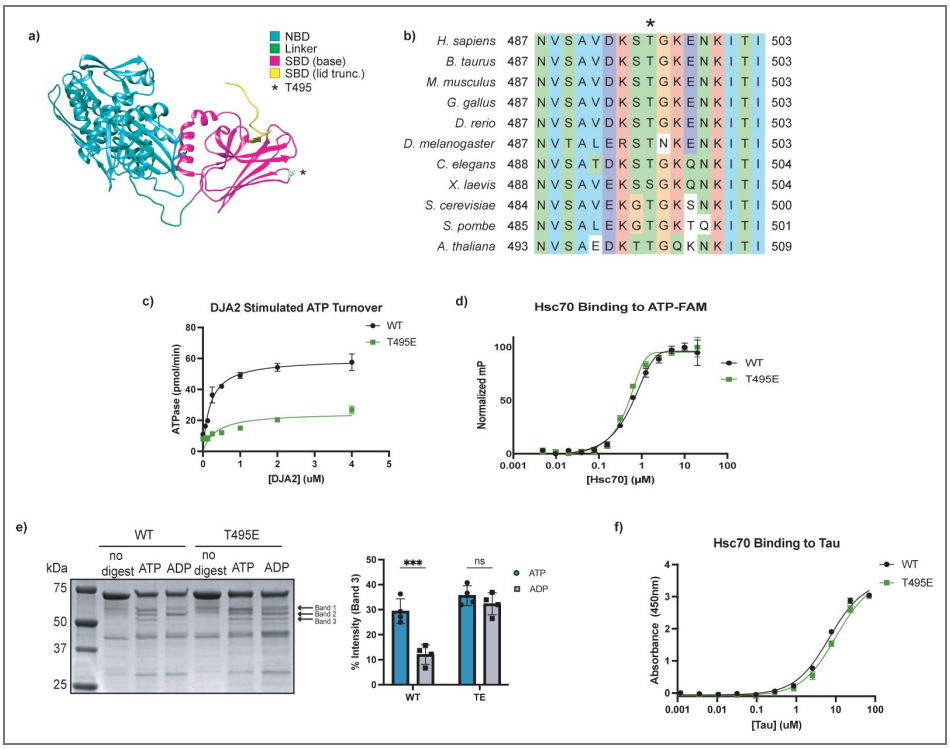

Figure 1. The phosphomimetic Hsc70 T495E mutant adopts an open-like conformation

a) Crystal structure of bovine Hsc70(residues 1-554; PDB: 1YUW). The nucleotide-binding domain (NBD, residues 1-383) is shown in cyan, the interdomain linker (residues 384-394) in green, and the substrate binding domain (SBD, residues 395-506) in magenta. T495 is highlighted in white and marked with an asterisk. **b)** Multiple sequence alignment of cytosolic Hsp70 orthologs. Human (P11142), mouse (P63017), cow (P19120), chicken (O73885), zebrafish (Q90473, fruit fly (P11147), worm (P09446), budding yeast (P10591), fission yeast (Q10265), and *Arabidopsis* (P22953) Hsc70 UniProt sequences were aligned with MAFFT (v7). Coloring follows CLUSTAL conventions; T495 is marked with an asterisk (*). **c)** J-protein-stimulated ATPase activity of wild-type (WT) and phosphomimetic Hsc70 (T495E) measured by malachite green assay. Data points represent mean + SD of technical triplicates. **d)** Fluorescence polarization of ATP-FAM binding to WT and T495E Hsc70. Values were normalized to the minimum and maximum polarization; data points represent mean + SD of technical triplicates. **e)** Partial proteolysis of WT and T495E Hsc70 by trypsin in the presence of ATP or ADP. Digestion products were resolved by SDS-PAGE and visualized with a Coomassie stain, and band intensities were quantified (bar graph, right). Statistical significance was determined by two-way ANOVA with Šidák's multiple comparisons test (adjusted p = 0.0002, n = 4 technical replicates). **f)** Tau binding to immobilized WT and T495E Hsc70 measured by ELISA. Data points represent mean + SD of technical triplicates.

Hsp70 chaperone activity is driven by cycling through nucleotide-dependent conformations[1]. In the ATP-bound state, Hsp70s adopt an 'open' conformation, and ATP hydrolysis to ADP induces large-scale structural rearrangements to a 'closed' state[1]. As T495E poorly hydrolyzes ATP, we reasoned that this mutation may lock the protein into either the open or closed conformation. Indeed, AMPylation of BiP at the analogous residue is known to lock the protein in an open state[17]. To assess the conformation of T495E Hsc70, we performed partial proteolysis using trypsin, which produces distinct cleavage patterns depending on the protein's conformation[18,19]. As expected, WT Hsc70 displayed nucleotide-dependent banding: protection of band 2 and loss of band 3 in the presence of ADP compared to ATP. In contrast, T495E exhibited an ATP-like banding pattern regardless of nucleotide, consistent with a locked open conformation (Figure 1e). While this agrees with the studies on BiP AMPylation, our previous work showed that phosphorylation coincides with increased occupancy of Hsc70 on polysomes, suggesting continued substrate engagement[13]. We therefore asked whether T495E can still bind client proteins. An ELISA with tau, a known Hsc70 substrate[20], showed that T495E retains the ability to bind tau despite the conformational lock (Figure 1f). These results suggest that T495E locks Hsc70 in a pseudo-open conformation: structurally similar to the ATP-bound open state in terms of protease sensitivity and domain exposure, yet still capable of substrate engagement typically associated with the closed state.

Base excision repair leads to Hsp70(T495) phosphorylation

Pathogens often mimic host proteins and hijack cellular pathways to create a favorable niche for replication. Thus, these pathogen-driven modifications frequently reveal biologically significant regulatory nodes within host systems[21]. Given this tendency of pathogens and the high degree of conservation of T495 (Figure 1b), we reasoned that *L.p.* phosphorylation of Hsp70 may be targeting an important regulatory module. Motivated by this concept, we examined published phospho-proteomics datasets to determine if this phosphorylation had been previously observed in eukaryotes. A phospho-proteomics study in *S. cerevisiae* identified phosphorylation at the analogous residue, Ssa1(T492), after treatment with the alkylating agent methyl methanesulfonate (MMS)[14]. Inspired by this finding, we analyzed human cells treated with MMS and observed that this phosphorylation is conserved(Figure 2a). As expected, this band is sensitive to phosphatase activity (Figure S1a).

This finding suggested that phosphorylation of Hsp70 might be involved in the response to DNA damage. MMS is primarily used as a DNA alkylating agent, though its chemical activity is not limited to DNA targets[22]. Thus, we sought to determine whether the response to MMS-induced DNA alkylation leads to Hsp70 phosphorylation. Aberrant DNA alkylation is predominantly repaired through the base excision repair (BER) pathway[23]. In BER, DNA glycosylases recognize and excise damaged bases, producing an abasic site (AP site). MMS-induced lesions are processed by N-methylpurine DNA glycosylase (MPG)[23,24] (Figure 2b). The backbone at the AP site is then cleaved by the endonuclease APE1, and the resultant single stranded break is repaired by a variety of proteins, including the DNA polymerase Polβ[23] (Figure 2b). Interestingly, the predominant DNA adduct generated by MMS, 7-methylguanine, is not intrinsically cytotoxic, but spontaneously depurinates to a toxic and mutagenic intermediate and so requires rapid repair[25,26]. The repair intermediates generated by the BER pathway, however, are cytotoxic[25,27]. Because Polβ activity is rate limiting, overexpression of the glycosylase that initiates BER can lead to an accumulation of these cytotoxic intermediates[23,28]. To determine whether increased BER activity affects Hsp70 phosphorylation, we treated cells overexpressing MPG with MMS. MPG overexpression modestly increased MMS-induced pHsp70 levels (Figure 2c). Conversely, inhibition of the subsequent BER step strongly reduced the levels of MMS-induced pHsp70. Pharmacological inhibition of APE1 led to a dose dependent decrease in Hsp70 phosphorylation (Figure 2d). Similarly, treatment with methoxyamine (Mx), which covalently binds AP sites and impairs APE1 cleavage and Polβ activity[29], caused a striking reduction in pHsp70 levels (Figure 2b,e). Surprisingly, overexpression of APE1 did not enhance pHsp70 (Figure S1b), suggesting that APE1 activity is necessary but not rate-limiting in this context. Additionally, overexpression of Polβ did not reduce

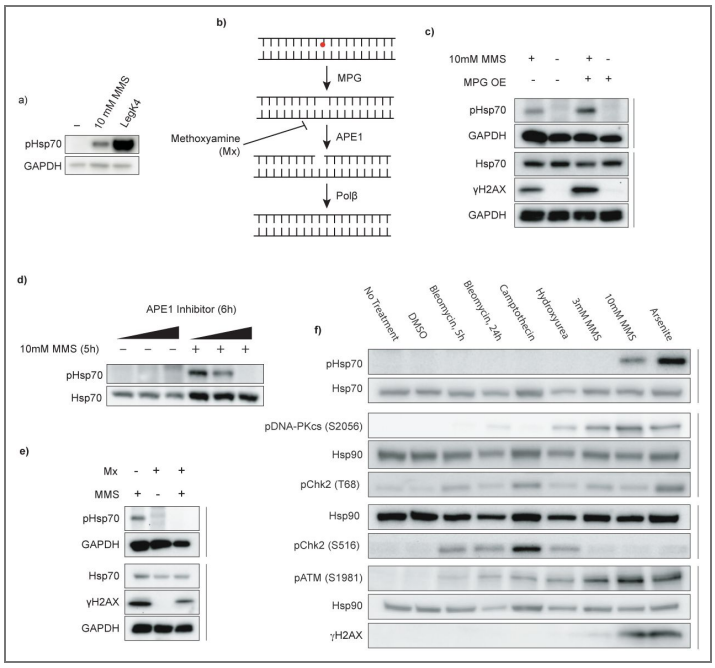

Figure 2. Base excision repair drives phosphorylation of Hsp70 in human cells

a) Hsp70 phosphorylation by MMS treatment or LegK4 overexpression. HEK293T cells were transiently transfected overnight with LegK4Δ1-58:GFP or treated with 10 mM MMS for 5 h. Phosphorylation at T495 was detected using a phospho-specific antibody to pHsp70 T495; GAPDH was used as a loading control. Data are representative of n > 3 independent experiments. **b)** Schematic of the base excision repair (BER) pathway, highlighting steps relevant to MMS-induced DNA damage. **c)** MPG overexpression increases pHsp70 levels. HEK293T cells were transiently transfected with MPG overnight, treated with MMS, and analyzed by immunoblotting for pHsp70, the loading controls GAPDH and Hsp70, and the DNA damage marker γH2AX. Data are representative of n = 3 independent experiments. **d)** Inhibition of APE1 reduces MMS-induced pHsc70. Cells were pretreated for 1h with 5μM, 10 μM, or 50 μM APE1 inhibitor (APE1 compound III) before MMS treatment. Hsp70 and pHsp70 were detected by immunoblotting. Data are representative of n = 3 independent experiments. **e)** Masking of AP sites prevents pHsp70 accumulation. Cells were pretreated with 60 mM methoxyamine (Mx) for 30 min, followed by cotreatment with 30 mM Mx and 10 mM MMS for 5 h. pHsp70, the loading controls GAPDH and Hsp70, and the DNA damage marker γH2AX were detected by immunoblotting. Data are representative of n = 3 independent experiments. **f)** DNA damage specificity panel for pHsp70 induction. Cells were treated with bleomycin (10 μM, 5 h or 24 h), camptothecin (10 μM, 5 h), hydroxyurea (2 mM, 24 h), MMS (3 mM or 10 mM, 5 h), sodium arsenite (0.5 mM, 5 h), or DMSO vehicle (5 h). Immunoblotting was performed for pHsp70, DDR kinase activation markers (pDNA-PKcs S2056, pChk2 T68, pChk2 S16, pATM S1981), DNA damage marker γH2AX, and loading controls (Hsp70 and Hsp90). Data are representative of n = 3 independent experiments.

pHsp70 upon MMS treatment (Figure S1c). These data confirm that the DNA alkylation by MMS is responsible for Hsp70 phosphorylation in human cells, and the results specifically indicate that BER intermediates may trigger this response.

To test the specificity of Hsp70 phosphorylation in response to DNA damage, we treated cells with a panel of genotoxic compounds that activate distinct branches of the DNA damage response (DDR), including bleomycin (induces double stranded breaks), camptothecin (a topoisomerase I inhibitor), hydroxyurea (depletes the dNTP pool), MMS, and arsenite (generates reactive oxygen species). While activation of DDR kinases (pDNA-PKcs(S2056), pATM(S1981) pChk2(T68), pChk2(S516)), and an increase of the DDR marker γH2AX confirm DNA damage and response induction in the drug treatment conditions, pHsp70 was only observed following high-dose MMS treatment, and exposure to sodium arsenite (Figure 2f). Arsenite causes oxidative DNA damage that can be repaired through BER[23,30]. Surprisingly, arsenite has also been shown to both inhibit the activity of enzymes necessary for this pathway, including OGG (the oxidative glycosylase)[31], and decrease the levels of others (e.g. APE1 and Polβ) [32]. Despite this, we found that both treatment with Mx and inhibition of APE1 were still sufficient to prevent Hsp70 phosphorylation upon arsenite treatment (Figure S1d,e). These findings suggest that Hsp70(T495) phosphorylation is selectively triggered by repair intermediates generated during BER.

Phosphorylation of Hsp70 requires the DDR kinases ATM, DNA-PKcs, Chk2, and CK1

Ape1 activity generates cytotoxic adducts. Its endonuclease activity at abasic sites directly generates single stranded DNA breaks (SSBs)[33]. These SSBs can in turn convert to DSBs through two primary mechanisms: collision of a replication fork with the SSB[33–35]; or generation of SSBs in proximity on opposing strands of DNA[36]. In these cases, damaged DNA is sensed and a response subsequently mounted through DDR pathways. At the highest level, the varied branches of the DDR are controlled by three master kinases: ataxia-telangiectasia mutated (ATM), ataxia-telangiectasia and Rad3-related (ATR), and DNA-dependent protein kinase (DNA-PK). ATR orchestrates the response to SSBs, while ATM and DNA-PK direct DSB repair through homologous recombination (HR) and non-homologous end joining (NHEJ), respectively[37,38]. While this broadly describes the organization of the DDR, the apparent simplicity belies the fact that these master regulators induce varied and nuanced responses depending on the exact type and severity of DNA damage present[39–42].

To determine if DDR signaling contributes to MMS-induced Hsp70 phosphorylation, we performed siRNA-mediated knockdowns of these three master kinases. Among these, only knockdown of DNA-PKcs prevented Hsp70 phosphorylation (Figure 3a, Supp Figure 2a,b). Interestingly, while ATM knockdown had no effect, pharmacological inhibition of ATM decreased Hsp70 phosphorylation (Figure 3b). To rule out off-target effects, we tested two independent ATM inhibitors and observed a similar reduction in pHsp70 with both (Figure 3b). This discrepancy is consistent with prior reports showing that genetic and pharmacological inhibition of ATM can yield diverging results[43,44]. Pharmacological inhibition of DNA-PKcs confirmed the DNA-PKcs knockdown experiment (Figure 3c). Both DNA-PKcs and ATM phosphorylate the transducer kinase Chk2, activating it and promoting propagation of the DDR[45]. Inhibition of Chk2 also prevented Hsp70 phosphorylation (Figure 3c). Given that casein kinase 1 (CK1) has been previously reported to act in concert with Chk2 in the DDR[46], we tested its involvement and found that CK1 inhibition also suppressed Hsp70 phosphorylation (Figure 3d, Figure S2c). Inhibition of these kinases also prevented Hsp70 phosphorylation upon arsenite treatment (Figure S2d).

While these kinases appear to be necessary for Hsp70 phosphorylation, our data are more consistent with their involvement in upstream signaling rather than directly acting on Hsp70. We would further highlight that the delay in Hsp70 phosphorylation contrasts with canonical DDR signaling, which is initiated within minutes of damage induction,[47,48] pHsp70 only emerges after prolonged MMS exposure (Fig 3d). Indeed, we observed robust activation of DNA-PKcs, ATM and

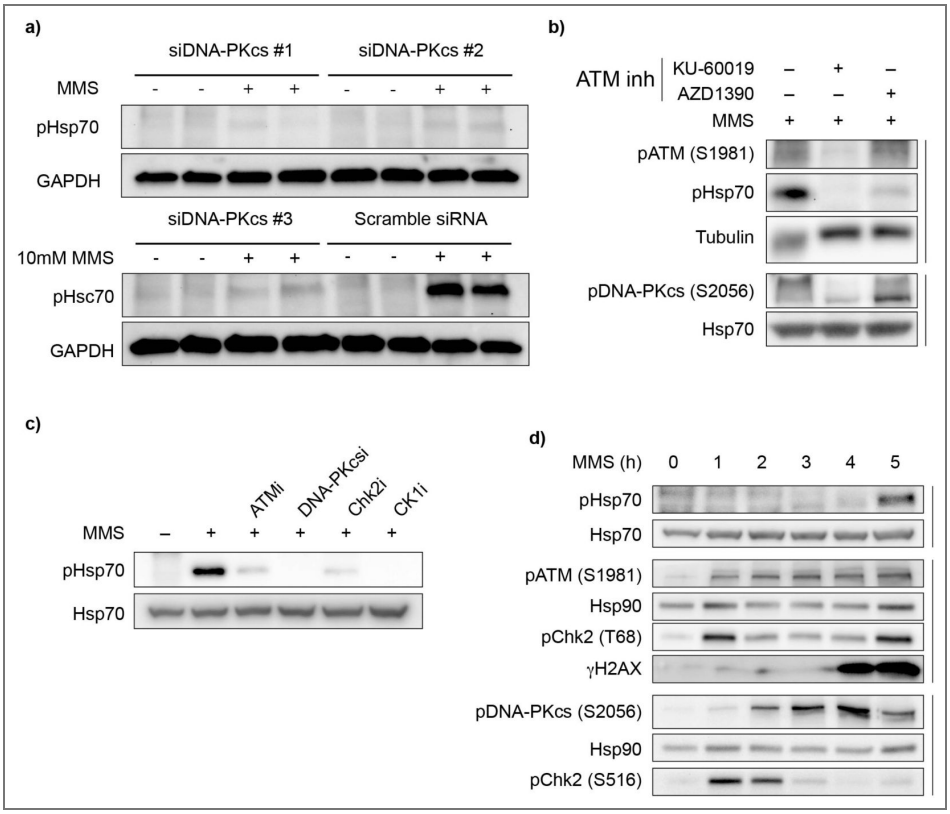

Figure 3. DDR kinase activity is upstream of Hsp70 phosphorylation

a) DNA-PKcs knockdown reduces pHsp70 levels. Cells were transiently transfected with three independent siRNAs targeting DNA-PKcs or a scramble control for 72 h, followed by treatment with 10 mM MMS for 5 h. pHsp70 and GAPDH (loading control) were detected by immunoblotting. Data are representative of n = 3 independent experiments. **b)** Pharmacological inhibition of ATM decreases pHsp70 induction. Cells were pretreated for 1 h with ATM inhibitors (10 μM KU-60019 or 200nM AZD1390), then treated with 10 mM MMS for 5 h. ATM and DNA-PKcs autoactivation were monitored by immunoblotting pATM (S1981) and pDNA-PKcs (S2056), respectively. Tubulin and total Hsp70 served as loading controls. Data are representative of n = 3 independent experiments. **c)** Pharmacological inhibition of ATM, DNA-PKcs, Chk2, and CK1 decrease Hsp70 phosphorylation during MMS treatment. Cells were pretreated for 1h with inhibitors for ATM (200 nM AZD1390), DNA-PKcs (2 μM AZD7648), Chk2 (5 μM CCT241533), CK1(50 μM PF-670462) or with vehicle control (DMSO), then treated with 10mM MMS for 5h. Immunoblotting was performed against pHsp70 and the loading control Hsp70. Data are representative of n = 3 independent experiments. **d)** Timecourse of MMS-induced DDR activation and pHsp70 phosphorylation. Cells were treated with 10 mM MMS and harvested hourly. ATM and DNA-PKcs activation were detected by pATM (S1981) and pDNA-PKcs (S2056), respectively. Chk2 activation was monitored by pChk2 (T68) and pChk2 (S516). DNA damage was assessed via γH2AX. Hsp70 and Hsp90 were used as loading controls. Data are representative of n = 3 independent experiments

Chk2 well before Hsp70 phosphorylation (Figure 3d). These observations raise the possibility that either prolonged MMS exposure or a secondary cellular response is required to trigger Hsp70 phosphorylation.

Hsp70 phosphorylation occurs after M phase onset

To better understand the timing of Hsp70 phosphorylation, we treated cells with MMS for varying durations (1 to 5 hours), followed by recovery in fresh media up to a total of 5 hours. In previous experiments, we observed robust Hsp70 phosphorylation only after 5 hours of continuous MMS treatment, with minimal signal at earlier timepoints (see Fig. 3d). However, in our pulse-chase assay, 2 hour MMS treatment, when followed by a 3 hour MMS-free chase, resulted in pHsp70 accumulation (Fig. 4a). This result indicates that prolonged MMS exposure alone does not fully explain the lag time between damage initiation and the appearance of pHsp70, suggesting that secondary cellular events or signaling contribute to Hsp70 phosphorylation.

Damage from MMS is thought to occur when replication forks collide with DNA repair intermediates in S phase[34,35]. This hypothesis, in combination with our observations that pHsp70 accumulation lags behind initial DDR activation, suggested that cell cycle stage might be a key determinant in Hsp70 phosphorylation. In asynchronous populations, Hsp70 phosphorylation might only appear when enough cells reach a permissive phase of the cell cycle. If this were true, synchronizing cells at the beginning of S phase should potentiate MMS-induced Hsp70 phosphorylation. To test this idea, we synchronized cells at the beginning of S phase using a double thymidine block, then released them into MMS-containing or untreated media. Unexpectedly, synchronization at G1/S does not increase Hsp70 phosphorylation (Figure 4b). Even more surprising, MMS-treated cells entered mitosis at an increased rate compared to controls, as evidenced by the accumulation of the mitotic marker phospho-Histone H3 (S10) (pH3), reduced levels of S phase markers such as the replication licensing factor CDT1 and thymidine kinase, and pCdk1 (Y15), the inhibited cyclin dependent kinase that must be de-phosphorylated for M phase entry (Figure 4b). These data suggest that MMS drives cells into mitosis, and that Hsp70 phosphorylation occurs after this transition. Indeed, blocking mitotic entry by treatment with a CDK1 inhibitor (Ro3306) prevented both MMS and arsenite induced Hsp70 phosphorylation (Figure 4c, Figure S3a). Releasing the CDK1 block upon MMS or arsenite treatment restored Hsp70 phosphorylation (Figure 4c, Figure S3a), suggesting this response does not require passage through S phase. While passage through mitosis upon DNA damage is necessary for Hsp70 phosphorylation, the presence of pHsp70 in a distinct nuclear fraction indicates that it persists after nuclear envelope reformation (Figure 4d). Indeed, a 2 hour pulse chase of MMS revealed that pHsp70 accumulates even after pH3 disappears, indicating that phosphorylation is maintained after mitotic exit (Figure 4e). Notably, we do not see an increase of S phase markers such as thymidine kinase, nor changes in cyclin A or cyclin B levels, suggesting that the cell cycle progression may be dysregulated following MMS treatment.

Phosphoregulation of Ssa1 at T492 is important for G1/S transition in yeast

To investigate the functional significance of Hsp70 phosphorylation at T495, we turned to *S. cerevisiae* due to its genetic tractability. *S. cerevisiae* has four cytosolic Hsp70s, Ssa1-4. Of these, Ssa1 and Ssa2 are constitutively expressed, whereas Ssa3 and Ssa4 are stress-inducible[49]. Phosphoproteomics studies revealed that Ssa1 can be phosphorylated at threonine 492, which corresponds to human Hsp70 T495[14,15]. To probe the role of this modification, we created phosphomimetic (T492E, TE) and phosphonull (T492A, TA) point mutations at the endogenous *SSA1* locus. Given the known redundancy between Ssa1 and Ssa2[50], we disrupted *SSA2* by inserting an antimicrobial resistance gene into its coding sequence to better assess the functional consequences of Ssa1 phospho-variants. To confirm the conservation of Hsp70 phosphorylation in yeast, we treated our mutants with MMS as previously described[14] and performed a Western blot. Notably, we see faint pHsp70 signal in WT yeast in the absence of MMS treatment (Figure 5a). This corresponds with prior work indicating low levels of phospho-Ssa1 (T492) in asynchronously

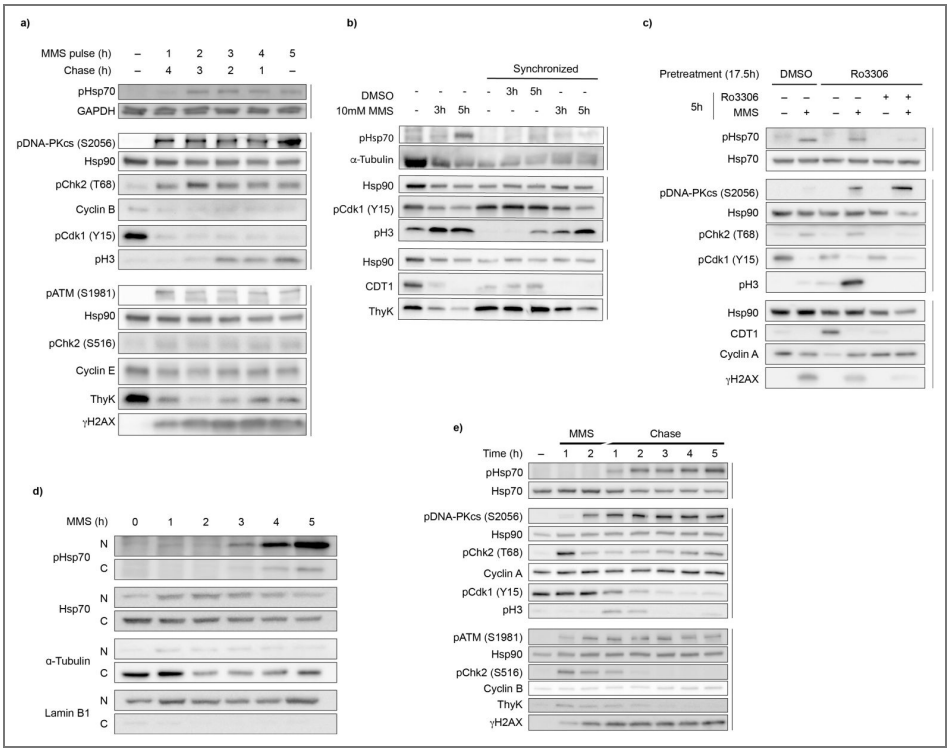

Figure 4. Hsp70 phosphorylation is linked to the cell cycle

a) Variable pulse-chase MMS treatment suggests a complex signaling pathway. Cells were treated with 10 mM MMS for 1-5 h, washed, then incubated in MMS-free media for the remainder of the 5 h period. ATM and DNA-PKcs activation were detected by pATM (S1981) and pDNA-PKcs (S2056); Chk2 activation by pChk2 (T68) and pChk2 (S516); DNA damage by γH2AX. Cell cycle progression was monitored with S phase markers thymidine kinase (ThyK) and CDT1; mitotic entry marker pCdk1(Y15) (dephosphorylation permits M-phase entry), M phase marker phospho-histone H3 (S10) (pH3); and cyclins B and E. GAPDH and Hsp90 are loading controls. Data are representative of n = 3 independent experiments. **b)** Early S-phase synchronization fails to increase pHsp70 accumulation. Cells were synchronized with 2.5 mM thymidine (18 h → 9 h release → 17 h retreatment), and released into fresh media ±10 mM MMS for the indicated times. Asynchronous cells were also MMS treated. Immunoblots were performed for pHsp70, cell cycle markers (pCdk1 Y15, pH3, CDT1, ThyK), and loading controls α-tubulin and Hsp90. Data are representative of n = 2 independent experiments. **c)** G2/M stalling by CDK1 inhibition reduces pHsp70 levels. Cells were pretreated with 10 μM CDK1 inhibitor Ro3306 or DMSO for 17.5 h, washed, then treated again with Ro3306 or DMSO ±10 mM MMS for 5 h. Immunoblotting was performed for pHsp70, cell cycle markers(pCdk1 Y15, pH3, CDT1, cyclin A), DDR markers (pDNA-PKcs S2056, pChk2 T68, γH2AX), and loading controls Hsp70 and Hsp90. Data are representative of n = 3 independent experiments. **d)** Subcellular fractionation of pHsp70 during MMS treatment shows nuclear localization. Cells were treated with 10 mM MMS from 1-5 h or left untreated. Cytoplasmic and nuclear extracts were prepared using the NE-PER kit. Immunoblotting was performed for pHsp70 and total Hsp70 levels; α-tubulin and lamin B1 served as cytoplasmic and nuclear markers, respectively. Data are representative of n = 3 independent experiments. **e)** A 2 h MMS pulse chase reveals pHsp70 accumulation post-mitosis. Cells were treated with 10 mM MMS for 2 h, washed, and then incubated in fresh media. Samples were harvested hourly, alongside an untreated control. Immunoblotting was performed for pHsp70, DDR markers (pDNA-PKcs S2056, pChk2 T68, pATM S1981, pChk2 S516, γH2AX), cell cycle markers (cyclin A, pCdk1 Y15, pH3, cyclin B, ThyK), and loading controls Hsp70 and Hsp90. Data are representative of n = 3 independent experiments.

growing cells.[15] This signal is diminished in the phosphomutant strains, and in all *ssa2Δ* strains, both supporting the conclusion that our antibody binds pHsp70(T492) in yeast, and indicating that there is likely redundant phospho-regulation of Ssa2 as well. Additionally, we find that MMS treatment leads to a strong increase in Hsp70 phosphorylation in WT, and phosphorylation to a lesser extent in WT;*ssa2Δ* (Figure 5a). Strikingly, even in the *SSA2* background, we observed a growth defect in TE yeast (Figure 5b,c). This is not likely explained by hypomorphism, as neither the TA mutant nor the WT;*ssa2Δ* strains show such a defect. Rather, phosphomimetic Ssa1 seems to act in a dominant-like manner. In the *ssa2Δ* background, strains expressing either phosphomimetic or phosphonull Ssa1 grew more slowly than the wild-type (Figure 5 b,c).

Phosphorylation of Ssa1 at T492 was previously reported to occur in a cell cycle dependent manner, specifically when yeast are prevented from exiting mitosis through the expression of a non-degradable cyclin B[15]. This information, in conjunction with the cell cycle dependence of pHsp70 in human cells and the growth defects we observed in our yeast phosphomutants, led us to examine the impact of these mutations on cell cycle progression. With SSA2 present, the Ssa1 WT and phosphonull (TA) strains showed similar cell cycle distributions. In contrast, the phosphomimetic mutant (TE) showed an increase in cells with 1N DNA content, consistent with a G1 stall (Figure 5d). In the *ssa2Δ* background for both Ssa1 WT and TA, we see a slight increase in the G1 population compared to G2, and the difference is even more pronounced in T492E yeast (Figure 5d). T492A yeast showed increased cell size in G1 in the *ssa2Δ* background, a phenotype previously linked to G1/S stalling, perhaps due to decreased Cln3 stability or disrupted Cln3-Ssa1 interactions[4,51] (Figure S3a). Intriguingly, both *ssa2Δ* point mutants exhibited a large cell size in G2/M (Figure S3a) — a finding that warrants additional investigation. Together, these data suggest that dynamic phospho-regulation of Ssa1 at T492 is critical for proper cell cycle progression.

We were curious if this modification served a similar cell cycle regulatory function during MMS treatment. To assess the overall viability of the point mutants in response to alkylation damage we performed a spot test in the presence and absence of MMS. In the *ssa2Δ* background, both phosphonull and phosphomimetic Ssa1 led to impaired growth on MMS-containing media, though growth in the in the *SSA2* background was only mildly impacted (Figure 5e). To examine how these mutations influence cell cycle progression in response to MMS, we treated the strains with 0.05% MMS for three hours as previously shown to cause Ssa1 phosphorylation at T492[14], and released them into fresh YPAD for the indicated times (Figure 5f). Ssa1 WT strains with and without *SSA2* behave similarly: immediately after the MMS treatment the cells display a bimodal distribution around G1 and early S. Upon MMS release, the G1 peak gradually disappeared, accompanied by synchronized progression through S phase, with DNA content slowly increasing over time. In the *SSA2* background, the T492A was nearly indistinguishable from the WT strains. However, in the *ssa2Δ* background, T492A no longer exhibited the bimodal distribution of cells near 1N immediately after MMS treatment. Rather, there was a single peak. Upon release, the cells failed to undergo coordinated S phase progression. Instead, DNA content increased in an asynchronous manner, suggesting impaired checkpoint regulation. The T492E mutants also showed distinct phenotypes. In the *SSA2* background, T492E cells lacked the bimodal distribution around 1N immediately after MMS treatment, and instead exhibited a more pronounced G1 arrest. Upon release, these cells progressed through S phase more slowly than WT, with a prominent left shoulder, indicating delayed DNA replication in a subset of cells. In the *ssa2Δ* background, the phenotype was even more prominent. A strong 1N peak persisted after MMS release, with minimal evidence of bulk S phase progression. Instead, we observed a gradual increase in DNA content across the population, reminiscent of the T492A mutant in *ssa2Δ*, but with a key difference: while T492A;*ssa2*Δ cells showed more rapid entry to and passage through S phase, T492E;*ssa2Δ* cells retained a distinct 1N peak and slower S phase progression. These data indicate that both phosphonull and phosphomimetic mutations disrupt the coordination of cell cycle re-entry following genotoxic stress. Loss of phosphorylation appears to weaken G1 arrest and promote uncontrolled S-phase entry, while constitutive phosphorylation reinforces arrest but impairs orderly progression through S-phase. Eliminating the functional redundancy of Ssa2 in the T492A;*ssa2*Δ and T492E;*ssa2*Δ strains reveals the importance of dynamic Ssa1 phospho-regulation

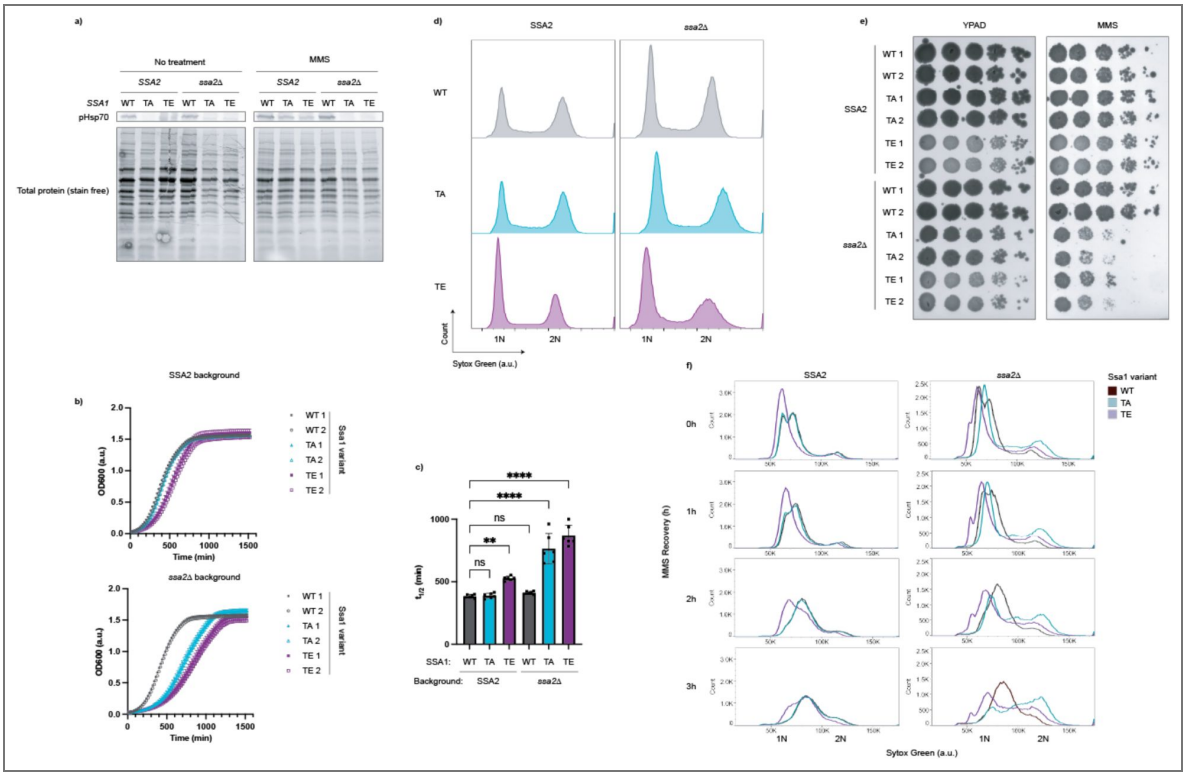

Figure 5. Ssa1 T492 phosphorylation mutations cause cell cycle defects in *S. cerevisiae*

a) Phosphorylation of Hsp70 is conserved in yeast. Strains were grown to mid-log and treated with 0.05% MMS in YPAD or fresh YPAD for 3 h. Immunoblots were performed for pHsp70 and total protein (StainFree, BioRad) was used as a loading control. Data are representative of n = 2 experiments. **b)** Growth curves of *S. cerevisiae* Ssa1 mutants show delayed growth. Indicated strains were grown to mid-log phase, diluted to the same starting concentration, and monitored overnight at 30 °C in a plate reader. Data represent the average of technical triplicates. Data are representative of n = 3 independent experiments. **c)** Half-times ($t_{1/2}$) of both Ssa1 mutants in the *ssa2Δ* background, and of the phosphomimetic mutant in the *SSA2* background, are significantly increased. Sigmoidal fits were applied to growth curves to determine $t_{1/2}$ values. The data represent three technical replicates with two biological replicates per strain. Bars represent mean + SD of six replicates (n = 6; 2 biological replicates x 3 technical replicates) Statistical significance was determined by ordinary one-way ANOVA followed by Dunnett's multiple comparison test (** p = 0.0015; **** p < 0.0001). **d)** Cell cycle distribution analysis reveals G1 stalling of Ssa1 phosphomutants. Yeast were grown to mid-log phase, adjusted to the same concentration, and immediately fixed. Cells were stained with Sytox Green and analyzed by flow cytometry to determine DNA content. Histograms display DNA content (X-axis) with 1N corresponding to G1 phase, 2N to G2/M, and intermediate values to S phase. Left: WT *SSA2* background; right: *ssa2Δ* background. Data are representative of n = 4 technical replicates with 2 biological replicates per strain. **e)** Ssa1 phosphomutants display increased MMS sensitivity in a spot test assay. Yeast were grown to mid-log phase, adjusted to 2e7 cells/mL, serially diluted 1:10, and spotted (5µL) onto YPAD plates with or without 0.0095% MMS. Plates were incubated at 30 °C and imaged after 3 days. Data are representative of n = 3 independent experiments. **f)** Ssa1 phosphomutants exhibit perturbed G1/S stalling during MMS recovery. Yeast were grown to mid-log phase, treated with 0.05% MMS for 3 h, washed, and resuspended in fresh media for recovery. Samples were collected at the indicated times points and analyzed by staining and flow cytometry as described as in (d). Data are representative of n = 2 technical replicates with 2 biological replicates per strain.

in mounting an effective DNA damage response and ensuring proper cell cycle transitions, as both phosphonull and phosphomimetic Ssa1 variants result in cell cycle dysregulation and altered growth in the absence of Ssa2.

Discussion

Our work demonstrates that Hsp70s are phosphorylated at T495 as part of a conserved response to DNA damage, and that dynamic phosphoregulation of this residue exerts control over the cell cycle. While prior phosphoproteomics studies in yeast detected phosphorylation of the analogous residue in Ssa1 (T492) following MMS exposure[14] or mitotic exit block[15], our findings establish that this modification is a regulated, damage-responsive event that is conserved in human cells. We show that phosphorylation is induced by two chemically distinct DNA-damaging agents, MMS and sodium arsenite, both of which generate BER substrates. Critically, inhibition of the BER endonuclease APE1 or chemical blockade of abasic site recognition and repair abolishes pHsp70 formation. Of note, high doses and long treatment times are required to elicit Hsp70 phosphorylation with both compounds, which raises questions as to the precise driver of this response. One caveat to this lies in our bulk detection method: the use of whole-cell lysate for Western blotting seems to dilute pHsp70 signal at earlier time-points, such that longer MMS treatment is required for sufficient pHsp70 to accumulate. This is illustrated by the fact that pHsp70 appears earlier in nuclear fractions that in whole-cell lysate (Figures 4d, 3d). While it is important to keep this limitation in mind, the dose and timing of insult still merits consideration. BER is a streamlined pathway: it is thought to follow a 'baton-passing' model, with each enzyme passing off intermediates to the next in the cascade[52]. However, BER intermediates are cytotoxic. APE1-mediated cleavage of the DNA backbone produces single-strand breaks that, if encountered by replication forks, can be converted into double-stranded breaks (DSBs)[34,35]. The requirement for APE1 activity, along with the involvement of the DSB repair kinases ATM and DNA-PKcs, support a model in which BER-induced DSBs lead to Hsp70 phosphorylation. While it is true that pharmacological inhibition and siRNA-mediated knockdowns can have off target and pleiotropic effects[53,54], our use of orthogonal approaches to perturb the aforementioned pathways in conjunction with knowledge that both MMS and sodium arsenite generate lesions repaired by BER leads us to believe that the parsimonious explanation is that phosphorylation of Hsp70 is downstream of a DNA damage response[23,24,30].

While it is clear that Hsp70 is phosphorylated in response to DNA damage, the lag time between insult and pHsp70 suggests a complex signaling pathway. Phosphorylation does not arise simply during damage exposure; instead, it requires both prolonged insult and progression through mitosis. Despite the longstanding view that MMS-induced damage primarily arises during S phase, we find that synchronizing cells at G1/S does not enhance Hsp70 phosphorylation. This paradox may be resolved by emerging evidence that BER-induced DSBs can occur in non-replicating cells[36]. Considering that the DDR is considerably rewired during mitosis, and though BER occurs, repair of lesions such as DSBs is forestalled until mitotic exit[41,55,56], it is possible that pHsp70 arises in response to high lesion burden in M phase to prevent cell cycle entry into the vulnerable S phase.

Our genetic studies in yeast directly link phosphoregulation of Ssa1 at T492 to cell cycle progression. Both phosphonull (T492A) and phosphomimetic (T492E) mutants cause growth defects in the absence of the compensatory isoform Ssa2, underscoring the importance of dynamic, reversible phosphorylation at this site. Alternatively, it is possible that the phosphonull mutation is not neutral and thus exhibits additional affects. Future work should examine the biochemical consequences of this mutation to clarify our findings. Cell cycle profiling reveals that T492E yeast in both *SSA2* and *ssa2Δ* backgrounds accumulate in G1 and fail to efficiently enter S phase following MMS exposure, while T492A strains show delayed recovery in the absence of Ssa2. Further, in the absence of MMS insult, the Ssa1 T492E mutant strain exhibits altered growth and cell cycle progression even in the *SSA2* background, suggesting a dominant-like effect of the phosphomimetic variant. The dominant-like phenotype of T492E is consistent with biochemical data suggesting persistent, aberrant substrate engagement, akin to the effects of mutations that

trap Hsp70 in a closed conformation[57]. Together, these results support a model in which pHsp70 serves as a reversible molecular brake, preventing premature S-phase entry under conditions of BER stress.

Interestingly, this mechanism parallels, but is distinct from the previously described phospho-Ssa1 (T36) mediated regulation of the cell cycle. Phosphorylation at T36/38 also enforces G1/S arrest in yeast. However, the residue is in the NBD, and phosphorylation decreases nucleotide binding. Furthermore, the activity is ER-localized, where it slows the accumulation of Cdk1-Cln3 by sequestering and promoting the degradation of Cln3[4]. In contrast, pT492/495 occurs in the SBD, modulates ATP hydrolysis without preventing nucleotide binding, and occurs in the nucleus. Given the established role of phosphorylation in directing Hsp70-client fate[58,59,67], it is plausible that pT492/T495 controls the stability or activity of nuclear substrates critical for G1/S transition. Our data support a model wherein Hsp70 engagement with both a client and some accessory machinery (e.g. a cochaperone) are controlled by phosphorylation to regulate S phase entry. For instance, if a specific Hsp70 client must be degraded to exit G1, phosphorylation may promote engagement with said client and proper degradation machinery, and dephosphorylation could allow client release. In this case, the phosphomimetic Hsp70 would be unable to disengage, and therefore cause the G1/S stall we report. Conversely, the phosphonull Hsp70 would be unable to establish proper interactions with the client and/or accessory machinery, thereby preventing efficient degradation and leading to the observed dysregulation of S phase re-entry. While this model explains our experimental observations, other possibilities remain, and future work is required to further establish mechanistic details.

Collectively, our findings reveal a conserved phospho-switch on Hsp70 that links DNA damage sensing during BER to cell cycle control, adding an unanticipated regulatory layer to the integration of repair and checkpoint pathways. Strikingly, this pathway came to light because it is targeted by a pathogenic effector kinase, once again illustrating how pathogens can hijack, and thereby illuminate, fundamental aspects of cell biology. Such examples underscore the enduring value of pathogens as powerful tools to uncover deeply conserved regulatory mechanisms. This work opens the door to identifying the upstream kinase(s) and downstream client(s) that mediate this effect, and to determining whether T495 phosphorylation serves as a general mechanism for coordinating repair with proliferation in diverse physiological contexts. By coupling BER to a reversible molecular brake on S phase entry, phosphorylation of Hsp70 at T495 emerges as a conserved checkpoint signal that safeguards genome integrity under conditions of repair-induced stress.

During the revision of this manuscript, Omkar et al. reported heat shock–induced phosphorylation of this residue in *S. cerevisiae* via the Cell Wall Integrity (CWI) pathway,[66] consistent with the regulatory potential we describe here.

Methods

Key resources

Plasmids

Description	ID	Source
Hsc70 in pMCSG7	pSM226	Moss 2019[13]
Hsc70(T495E) in pMCSG7	pSM227	Moss 2019[13]
LegK4Δ1-58 in pEGFP-C2	pSM160	Moss 2019[13]
MPG in pIRESNeo	pSM282	Addgene Plasmid #12548
APE1 in pCMVd3	pSM303	This study
pCMVd3 empty vector	pSM304	This study
Polβ in pLVX-GWE-IRES-puro	pSM288	Addgene Plasmid #128653
plVX-GWE-IRES-puro empty vector	pSM289	This study
pYM13 PCR template KanMX resistance	pSM302	Gift from David O. Morgan Lab

RNA Oligos

Description	Sequence
siDNA-PKcs #1	GCGUUGGAGUGCUACAACA[dT][dT]
siDNA-PKcs #2	CAAGCGACUUUAUAGCCUU[dT][dT]
siDNA-PKcs #3	GACCCUGUUGACAGUACUU[dT][dT]
siATM #1	GCUGUUACCUGUUUGAAAA[dT][dT]
siATM #2	CACCUGUUUGUUAGUUUAU[dT][dT]
siATM #3	CAGCUGUCAUCAUAUAAGA[dT][dT]
siATR #1	GAGCCGAUUUUUAAGUCAA[dT][dT]
siATR #2	GAUGAGUAUGCAAAAUUUA[dT][dT]
siATR #3	GCCGCUAAUCUUCUAACAU[dT][dT]

DNA Oligos

Description	Sequence
SSA1 gDNA T492E Forward	TCGATGTCGACTCTAACGGTATTTTGAATGTTTCCGCCGTCGAAAAGGGTGAAGGTAAGTCTAACAAG
SSA1 gDNA T492A Forward	TCGATGTCGACTCTAACGGTATTTTGAATGTTTCCGCCGTCGAAAAGGGTGCTGGTAAGTCTAACAAG
SSA1 gDNA Reverse	CAGATCATTAAAAGACATTTTCGTTATTATCAATTGCCGCACCAATTGGCGCATGCCGGTAGAGG
SSA2-KanMx Forward	TTGATTAATTCCAACAGATCAAGCAGATTTTATACAGAAATATTTATACAATGGGTAAGGAAAAGACTCA
KanMx-Ssa2 Reverse	GGAAAGCAAAAGTAAAACTTTTCGGATATTTTACAGGGCGATCGCTAAGCTTAGAAAAACTCATCGAGCA

Antibodies

Antigen	Dilution	Supplier (catalog #)
pHsp70	1:5000	Custom (Moss 2019)[13]
GAPDH	1:3000	Proteintech (60004-1-Ig)
γH2AX	1:1000	Millipore Sigma (05-636)
Hsp70	1:1000	Santa Cruz Biotechnology (sc-66048)
pDNA-PKcs (S2056)	1:1000	Abcam (ab18192)
pChk2 (T68)	1:1000	Cell Signaling Technology (2197T)
Hsp90	1:1000	Cell Signaling Technology (4874S)
pChk2 (S516)	1:1000	Cell Signaling Technology (2669T)
pATM (S1981)	1:1000	Cell Signaling Technology (4526S)
Tubulin	1:3000	Proteintech (66031-1-Ig)
Thymidine Kinase	1:1000	Cell Signaling Technology (28755S)
pCdk1 (Y15)	1:1000	Cell Signaling Technology (4539S)
Cyclin B	1:500	Santa Cruz Biotechnology (sc-245)
pHistone H3 (S10)	1:1000	Cell Signaling Technology (53348S)
Cyclin E	1:1000	Santa Cruz Biotechnology (sc-247)
CDT1	1:1000	Cell Signaling Technology (8064S)
Lamin B1	1:1000	Proteintech (12987-1-AP)
Cyclin A	1:1000	Santa Cruz Biotechnology (sc-271682)
Polβ	1:1000	Proteintech (18003-1-AP)
APE1	1:1000	Proteintech (10203-1-AP)
ATM	1:1000	Cell Signaling Technology (2873S)
ATR	1:1000	Cell Signaling Technology (2790S)

Yeast Strains

Description	ID
Parental W303α	Y017
Ssa1(WT)-NAT #1	Y019
Ssa1(WT)-NAT #2	Y034
Ssa1(T492A)-NAT #1	Y040
Ssa1(T492A)-NAT #2	Y041
Ssa1(T492E)-NAT #1	Y038
Ssa1(T492E)-NAT #2	Y039
Ssa1(WT)-NAT;*ssa2*Δ #1	Y023
Ssa1(WT)-NAT;*ssa2*Δ #2	Y037

Ssa1(T492A)-NAT;*ssa2*Δ #1	Y051
Ssa1(T492A)-NAT;*ssa2*Δ #2	Y046
Ssa1(T492E)-NAT;*ssa2*Δ #1	Y044
Ssa1(T492E)-NAT;*ssa2*Δ #2	Y057

Software (all code available upon request)

Software	Source	URL
Prism Version 10.4.2	Graphpad	https://www.graphpad.com/scientific-software/prism/
ImageLab 6.0.1	Biorad	https://www.bio-rad.com/en-us/product/image-lab-software?ID=KRE6P5E8Z
FlowJo™ 10.10.0	BD Life Sciences	https://flowjo.com/flowjo/download
UCSF Chimera X v1.3	Pettersen et al.[60]	https://www.rbvi.ucsf.edu/chimera

Cell Culture

HEK293T and HeLa lines were obtained from ATCC. All cell lines were regularly tested for mycoplasma contamination. Cells were maintained in Dulbecco's modified Eagle's medium (DMEM, Gibco) supplemented with 10% fetal bovine serum (FBS, VWR) in a humidified incubator at 37°C, 5% CO_2. Cells were treated with 10 mM methyl methanesulfonate (MMS) (Fisher AC156890050) for 5 h unless otherwise indicated. Cells were treated with methoxyamine hydrochloride (Sigma Aldrich 226904), APE1 compound III (EMD Millipore 262017), bleomycin (sulfate) (Thomas Scientific C830H18), camptothecin (Selleck S1288), hydroxyurea (Sigma-Aldrich H8627), sodium arsenite (Fisher Scientific S88733), KU-60019 (MedChem Express HY-12061), AZD1390 (MedChem Express 2089288-03-7), CCT241533 (MedChem Express HY-14715B), PF-670462 (Sigma-Aldrich SML0795), thymidine (Fisher 501882638), Ro-3306 (MedChem Express HY-12529), and AZD7648 (MedChem Express 2230820-11-6) as described in the figure legends.

siRNA and Plasmid Transfection of Mammalian Cells

Cells were transfected with high quality maxiprepped plasmid DNA (Sigma Genelute HP kit), custom synthesized siRNA duplexes (Sigma-Aldrich VC30002), or Mission® siRNA Universal Negative Control #1 (Sigma Aldrich SIC001) using the jetPRIME transfection system (VWR 89129-926). For plasmid transfection, cells were grown to 70% confluence and transfected overnight with total µg of DNA added as recommended by supplier for the culture vessel. For siRNA transfection, knockdowns were performed per manufacturer suggestions in HeLa cells. Cells were transfected for 24 h after which the media was replaced with fresh media. Cells were allowed to grow for an additional 48 h before any additional treatment and harvesting.

Whole Cell Lysate Preparation and Western Blotting

Once experimental manipulations were complete, media was aspirated and cells were washed 3X with ice cold 1X TBS on ice. Cells were gently scraped into 1 mL ice cold 1X TBS and transferred to 1.5 mL microcentrifuge tubes. Cells were pelleted at 3000xg for 5 min at 4 °C, and the supernatant was aspirated. Pellets were stored at -80 °C until lysis.

1x RIPA lysis buffer (Cell Signaling Technology 9806S) supplemented with 1x Roche cOmplete protease inhibitor cocktail (Roche 11697498001), 1x Roche PhosStop (Roche 04906837001) or 1x Halt Phosphatase Inhibitor Cocktail (Thermo Scientific 78440), and 1 mM PMSF was added to the frozen pellets which were then agitated for 30 min at 4 °C then centrifuged at 16,000 xg for 15 min at 4 °C. Cleared lysates were transferred to a new tube, and protein concentrations were quantified using the Pierce BCA Assay Kit (Thermo Scientific 23227). 30-100 µg total protein was denatured in 1x SDS sample buffer with 10mM dithiothreitol (DTT) for 8 min at 95 °C. Lysates were loaded onto polyacrylamide gels (8, 10% or Bio-Rad Mini-PROTEAN TGX Precast Protein Gels, 4-20%) (BioRad) and separated by SDS-PAGE. Proteins were transferred to methanol-activated 0.2 µm pore PVDF membranes overnight at 4 °C in 1X CAPS, 10% methanol. Membranes were blocked in either 5% bovine serum albumin (BSA) (VWR) for phopsho-specific antibodies, or 5% non-fat

dry milk (BioRad) in TBS-T (0.1% Tween-20 in TBS) for 1 h at RT. Primary antibodies were diluted in 5% BSA, 0.02% NaN_3 in TBS-T. Membranes were incubated with primary antibody solutions overnight at 4°C. Membranes were washed 3X in TBS-T for 10 min each wash, then incubated with 1:5000 secondary antibody in blocking buffer for 1 h at RT. Membranes were washed 3X in TBS-T for 10 min each wash, then developed for 1 min in Amersham ECL Western Blotting Detection Reagent (Cytiva RPN2209) or Immobilon Crescendo (Millipore WBLUR0500) and imaged on a ChemiDoc Imaging System (BioRad).

Phosphatase Sensitivity

HEK293T cells were treated with 10 mM MMS for 5h or left untreated. Following treatment, the cells were harvested and split into two 1.5 mL microcentrifuge tubes per condition. Cells were lysed in home-made RIPA buffer (20 mM Tris HCl pH 7.5, 150 mM NaCl, 1 mM EDTA, 1% Triton X-100, 1% sodium deoxycholate, 0.1% SDS) supplemented with 1 mM PMSF, 1x PhosStop (Roche 04906837001). The lysis buffer was further supplemented with 1x Roche PhosStop (Roche 04906837001) or 1x Halt Phosphatase Inhibitor Cocktail (Thermo Scientific 78440) for the '+ phosphatase inhibitor' samples. Lysis, protein quantification, and Western blots were performed as described above.

Nuclear and Cytoplasmic Extraction

Nuclear and cytoplasmic extraction was performed at 4 °C using the NE-PER Nuclear and Cytoplasmic Reagents (Fisher Scientific PI78835, Thermo Scientific 78833) following the manufacturer's protocol. Protein quantification and Western blotting was performed as described above.

Protein Purification

Hsc70 and point mutants were purified as described previously[61]. In brief, plasmids containing His-tag proteins were transformed into Rosetta(DE3) *E. coli*. Bacteria were grown in 2 L Terrific Broth (TB) to OD_{600}=0.6. Bacterial cultures were cooled to 20 °C, and protein expression was induced with 200μM IPTG at 20 °C overnight. The cells were harvested by centrifugation (7500 r.p.m. 10 min, JLA 8.1 rotor) and then resuspended in 20 mL His-Binding Buffer (50 mM Tris, 10 mM imidazole, 500 mM NaCl, pH 8) + 2 tablets EDTA-free Roche cOmplete Protease Inhibitor per liter culture using a Dounce homogenizer. Cells were then lysed by sonication at Amp 35% for 5 min, 30 sec on, 30 sec off, on ice at 4 °C. Lysate was separated by centrifugation (18000 r.p.m. 30 min, JA-20 Beckman rotor) and incubated with 10 mL/L pre-equilibrated Ni-NTA resin (EMD Millipore 70666-5)/liter of culture at 4 °C for 1 h. Bound protein was first washed with 200 mL His-binding buffer, then 100 mL His-Washing buffer (50 mM Tris, 30 mM imidazole, 300 mM NaCl, pH 8) , and then eluted with His-Elution buffer (50 mM Tris, 300 mM imidazole, 300 mM NaCl, pH 8). This His-tag was then removed by the spiking in 5 mM β-mercaptoethanol and 600 μg TEV protease to the sample and dialyzing overnight into Buffer A (25 mM HEPES, 5 mM $MgCl_2$, 10 mM KCl, pH 7.5) in 10 KDa MWCO snakeskin dialysis tubing (Thermo Fisher 68100). The protein was further purified by an ATP-agarose column using previously established protocols[61]. Purified DnaJA2 and tau were acquired from J.E.G.

ATPase Assays with Malachite Green

The ATPase activity of Hsc70 and Hsc70(T495E) was performed with malachite green (MG) (Sigma Aldrich) as described previously[62]. Briefly, in a clear 96-well plate, Hsc70 or Hsc70(T495E) were incubated with increasing concentrations of human DnaJA2 (DJA2) in 25 μL total volume. Reactions were also performed with DnaJA2 in the absence of Hsc70 for background subtraction. The assay buffer was 100 mM Tris at pH 7.4, 20 mM KCl, 6 mM $MgCl_2$, and 0.01% Triton. The reaction was initiated by the addition of ATP at a final concentration of 1 mM and incubated at 37 °C for 1 h. After incubation, 80 μL of MG reagent was added, followed by 10 μL of saturated sodium

citrate to quench the reaction. Absorbance was measured at 620 nm on a SpectraMax M5 plate reader (Molecular Devices). ATP hydrolysis rates were calculated by comparison to a phosphate standard. Displayed curves are a combination of 6 replicates.

Fluorescence Polarization (FP) of ATP-FAM

Nucleotide of Hsc70 and Hsc70(T495E) was assessed with a fluorescence polarization (FP) assay using labeled ATP. First, apo-Hsc70 was generated by subsequent 6-12h dialyses in the following buffers: buffer 1 (25 mM HEPES, 100 mM NaCl, 5 mM EDTA (pH 7.5)), buffer 2 (25 mM HEPES, 100 mM NaCl, 1 mM EDTA (pH 7.5)), buffer 3 (25 mM HEPES, 5 mM $MgCl_2$, 10 mM KCl (pH 7.5)). Following this, 40 kDa MWCO Zeba Buffer Exchange columns (Thermo Fisher A57760) were used to exchange the buffer to FP assay buffer 100 mM Tris, 20 mM KCl, 6 mM $MgCl_2$, pH 7.4) before protein quantification. The assay was performed in 384-well black round-bottom low-volume plates (Corning 4511). 40 nM ATP-FAM (Jena Bioscience nu-805-5fm) was added to each well for a final concentration of 20 nM in 20 µL. Hsc70 and Hsc70(T495E) were added for a starting concentration of 20 µM in 20 µL, and then serially diluted with FP assay buffer (2-fold 13 times into the ATP-FAM. Plates were covered and incubated for 30 min at room temperature. Fluorescence polarization was read on a SpectraMax M5 plate reader (excitation, 485 nm; emission, 535 nm)

Partial Proteolysis

The partial proteolysis protocol to identify Hsp70 conformations was modified from previous work[18]. Hsc70 and Hsc70(T495E) was buffer exchanged to proteolysis buffer (40 mM HEPES, 20 mM NaCl, 8 mM $MgCl_2$, 20 mM KCl, 0.3 mM EDTA, pH 8) using Zeba 40 kDa MWCO buffer exchange columns and diluted to 3 µM in this buffer. ATP or ADP was added to 1 mM and incubated for 30 min at room temperature. 1.5 µM trypsin (Sigma EC 3.4.21.4) was added for 2 h at room temperature. The reaction was quenched by boiling in SDS loading buffer (125 mM Tris-HCl pH 6.8, 5% SDS, 10% β-mercaptoethanol, 20% glycerol, 0.025% bromophenol blue), run on a precast SDS-PAGE gel (Bio-Rad) and stained by Coomassie.

Hsc70-tau binding ELISA

Hsc70-tau ELISA was modified from a previously published protocol[63]. It was performed in a Fisherbrand, Flat bottom 96-well plates, clear, PS (cat no 12565501). 1µM Hsc70 or Hsc70(T495E) (diluted in dialysis buffer 3 from FP assay) was added to wells along with 1 mM ATP and incubated overnight at 37°C. Protein was discarded from wells followed by 3x 3min washes on rocker with PBS-T, discarding the PBS-T and vigorously blotting the inverted plate on a paper towel between each wash. In triplicate, add 30 uL of tau to each well, spanning a 12-dose 3-fold concentration gradient (from 70 µM). Plates were covered and incubated at room temperature for 3 h. Solutions were removed and wells washed 3x with PBS-T as described above. 100 µL of blocking solution (5% non-fat milk in TBS-T) was added to all wells and incubated at room temperature for 5 min without rocking. Solution was removed without washing. 50 uL of primary antibody was added to all wells (1:2000 mouse anti-tau clone D-8 from SantaCruz Biotechnologies in blocking solution). The plate was incubated for 1 h at room temperature without shaking. Solution was removed and wells washed 3x with PBS-T. 50 µL of secondary antibody (1:2000 goat anti-mouse (Jackson 115-035-146)in blocking solution) was added to the wells. The plate was incubated for 1h at room temperature and then washed 3x with PBS-T. 50 µL of TMB substrate was added to the wells (ThermoFisher 34028) and incubated for 15 min at room temperature in the dark. 50 µL 1M HCl was added and the plate read at 450 nm on SpectraMax M5 plate reader.

Yeast Strain Generation

W303α yeast and W303α yeast with SSA1 NAT were gifted to us by David Morgan. Oligos for yeast point mutations were generated by PCR amplification of NAT-SSA1with the relevant codon substituted in the primer sequence. Oligos for SSA2 interruption were generated by PCR amplification of KanMX from pYM13 with flanking sequences to SSA2. gDNA was extracted from yeast by first suspending yeast colonies from a YPAD plate in 100 µL LiOAc/SDS buffer (0.2 M

LiOAc, 1% SDS). Cells were incubated at 70 °C for 10 min, and then 300 µL 96-100% ethanol was added. Sample was then mixed by vortexing. Sample was the spun at 15,000 xg for 3 min, supernatant removed, and pellet dissolved in 100 µL nuclease free water. The sample was then spun down at maximum speed for >15 sec, and supernatant was transferred to a new tube. 1 µL of supernatant was used for subsequent PCRs.

For yeast transformations, competent cells were generated by first diluting an overnight culture 1:20 in YPAD and grown on a rotary shaker at 30 °C to mid-log. The yeast were spun at 3000 xg for 1min. While spinning the yeast, 10 mg/mL salmon sperm DNA (Sigma-Aldrich D9156) was boiled for 5 min and then put on ice. The supernatant was removed from the yeast pellet which was then washed 1x in water and re-pelleted. The water was remove and the yeast was resuspended in LiOAc/TE solution (10 mM Tris-HCl pH 8, 1 mM EDTA, 0.1 M lithium acetate (Sigma-Aldrich L4158)). This was then pelleted, the supernatant aspirated, and yeast were resuspended in 200 uL LiOAc/TE solution to generate competent cells. For each transformation, 50uL of these competent cells were mixed with 1µg of DNA along with 10 µL of boiled salmon sperm DNA and 500 µL of PEG/LiOAc/TE solution (10 mM Tris-HCl pH 8, 1 mM EDTA, 0.1 M lithium acetate, 40% PEG 3350). This mix was incubated at 30 °C with shaking at 550 r,p,m, on a ThermoMixer F1.5 (Eppendorf), then spun for 1 min at 3000 xg. The supernatant was removed and the yeast resuspended in sterile water and plated on YPAD and grown overnight at 30 °C. The following day, these plates were replica plated onto plates with the appropriate selection marker.

Yeast Growth

For all yeast experiments, yeast were first grown overnight in YPAD on a rotary shaker at 30 °C. The following morning, yeast were diluted to OD_{600} =0.3 and grown at 30 °C to midlog (OD_{600} =~0.6). Strains were then concentrated (by centrifugation at 3000xg) to 2e7 cells/mL in 1.5 mL microcentrifuge tubes.

Growth Curve

The above yeast were diluted 1:30 into a clear flat bottom 96 well plate (Costar 3370) and grown for 25 h with continuous orbital shaking at 30 °C on a Cytation 5 Imaging Reader (BioTek) with OD_{600} collected every 20 min.

Yeast Spot Test

The day prior to the experiment, Nunc Rectangular Dishes (Thermo 267060) were made with either YPAD or YPAD + 0.0095% MMS. The above yeast were serially diluted 10-fold 5 times. 5 µL of the dilutions were spotted on the YPAD or YPAD + MMS plates. Plates were grown for three days at 30 °C and imaged daily on a ChemiDoc Imaging System (BioRad).

Yeast Cell Cycle Analysis

This protocol was modified from previous work[64,65]. For cell cycle analysis of yeast at mid-log, we took 500 µL of the 2e7 cell/mL yeast solution, spun it at 14,000 xg for 30 sec, removed the supernatant, washed 1x in water and re-pelleted. The water was then decanted, and the yeast were vortexed to resuspend them in the water remaining in the tube. 95% ethanol prechilled to -20 °C was added to the resuspended yeast which were then vortexed and placed on ice. For MMS treatment, yeast were grown to mid-log as previously described. 0.05% MMS (Fisher Scientific AC156890050) was then added to the yeast for 3 h[14], rotating at 30 °C. Samples were harvested as described for 'no recovery' conditions, and the remaining yeast was transferred to 15 mL centrifuge tubes (Fisher Scientific 12-565-268),spun at 300 xg. The pellet was washed 1x with sterile water, spun down again, and then resuspended in the starting volume of YPAD. The caps were partially unscrewed and the yeast was returned to the rotary at 30 °C with samples harvested as detailed above at the indicated time points. Once all samples were resuspended in ethanol the yeast were stored at -20 °C for at least overnight. The yeast were then resuspended by vortexing and spun at 14000 xg for 1 min. The ethanol was removed, the yeast resuspended in water and then pelleted again. The water was removed and the pellet was resuspended in 1mL

sodium citrate buffer (50 mM sodium citrate (C8532), pH to 7.5 with citric acid (BP399)). 8 µL of 10 mg/mL RNAase A (Thermo EN0531) was then added to the samples and incubated for 2 h at 37 °C. Following this, 10 µL of 20 mg/mL Proteinase K (NEB P8107S) was added to the samples and incubated for 1 h at 50 °C. The samples were then incubated at 4 °C overnight. The samples were spun down at 14000 xg for 1 min and the pellets resuspended in 500 µL sodium citrate buffer + 2.5 µM SYTOX Green (Thermo Fisher S7020), or sodium citrate buffer alone for the no-stain control. Samples were placed on ice and sonicated with a probe sonicator (QSonica) at 30% amplitude for 10 sec. The samples were then stored in the dark at 4 °C until flow cytometry analysis.

All yeast flow cytometry experiments were performed on a LSRII SORP (BD Biosciences) using a 488 nm laser, and the software analysis done on FlowJo (10.10.0). Cells were first selected by graphing FSC-A by SSC-A. Singlets were then gated by graphing FSC-A by FSC-H and then analyzed.

Yeast Lysis for Western Blotting

Yeast samples were treated as described, then 1 mL of sample was pelleted in a 1.5 mL microcentrifuge tube at 13,000 xg for 1 min, washed 1x in water, pelleted at 13,000 xg, and then the pellets were stored at -80 °C. The following day, the pellets were resuspended in 200 µL of 20% trichloroacetic acid (TCA). The samples were then centrifuged at 13,000 rpm for 30 sec at 4 °C. The supernatant was removed, and the pellets were washed with acetone prechilled in a - 20 °C freezer. The samples were spun at 13,000 rmp for 30 sec, the supernatant removed, and the samples allowed to airdry at RT for ~10 min or until fully dry. The pellets were then resuspended in 40 µL of 1M Tris pH 7.5, and then 200 µL of 2x Lamelli Buffer + 2% DTT was added to each sample. Using a 200 µL PCR tube (VWR 53509-304), ~400 µL of 0.5 mm glass disrupter beads (USA Scientific 7400-2405) were scooped into the sample and the sample was beaten vigorously for 90 sec. With a 25 gauge needle, carefully hole was poked in the bottom of the tube. The tube was then placed in a plastic vial (Falcon 352063), and spun with tops closed at 500 xg for 3 min. The flowthrough was transferred to clean 1.5 mL microcentrifuge tube and boiled for 10 min. Equal volumes of sample were then run in a 8-16% precast Mini-PROTEAN TGX Stain Free gel (Bio-Rad 456-8103) per the manufacturer protocol. The Western block was performed as described above.

Data Reproducibility and Statistical Analysis

All statistics were performed in Prism as described in the relevant figure legends. Figures are either mean + SD, or representative of the number of replicates described in the figure legend.

Data availability

We will make the data freely and widely available as needed

Acknowledgements

We thank Dr. David Booth, Dr. Adriana Steinbach, and Dr. Michael Metrick for critical evaluation and discussions of the data. We thank Dr. Henry Ng and Dr. David O. Morgan for yeast strains and technical advice. We thank Dr. Oleta Johnson, Dr. Cory Nadel, and Dr. Emma Carroll from the J.E.G. lab for technical assistance and advice. We acknowledge Vinh Nguyen for his technical support and the PFCC (RRID:*SCR_018206*) for assistance generating Flow Cytometry data. Research reported here was supported in part by the DRC Center Grant NIH P30 DK063720. T.M. acknowledges support from the MPHD T32 training grant. J.E.G. acknowledges support from R01NS059690. S.M. acknowledges financial support from the National Institutes of Health (grant nos. R01GM140440 and R01GM144378), the Pew Charitable Trust (grant no. A129837), a Bowes Biomedical Investigator award, and is a Biohub, San Francisco, Investigator.

Additional information

Author contributions

Conceptualization, T.M., S.M.; Experiment design, T.M., J.E.G., S.M.; Experimentation, T.M., A.W. K.B. M.C..; Formal Analysis, T.M..; Writing, T.M., S.M.; Review & Editing T.M, A.W., J.E.G., S.M.; Funding Acquisition: J.E.G., S.M.

Funding

Funder	Grant reference number	Author
HHS | NIH | National Institute of General Medical Sciences (NIGMS)	R01GM140440	Shaeri Mukherjee
HHS | NIH | National Institute of General Medical Sciences (NIGMS)	R01GM144378	Shaeri Mukherjee
HHS | NIH | National Institute of Neurological Disorders and Stroke (NINDS)	R01NS059690	Jason E Gestwicki

Author ORCID iDs

Thomas Moss: https://orcid.org/0000-0003-3647-9319
Jason E Gestwicki: https://orcid.org/0000-0002-6125-3154
Shaeri Mukherjee: https://orcid.org/0000-0003-3820-0174

Additional files

Supplemental Figures.

References

1. **Rosenzweig R.,** Nillegoda N. B., Mayer M. P., Bukau B (2019) The Hsp70 chaperone network. *Nat. Rev. Mol. Cell Biol* **20**:665-680 https://doi.org/10.1038/s41580-019-0133-3 | PubMed
2. **Kaushik S.,** Cuervo A. M (2018) The coming of age of chaperone-mediated autophagy. *Nat. Rev. Mol. Cell Biol* **19**:365-381 https://doi.org/10.1038/s41580-018-0001-6 | PubMed
3. **Dubrez L.,** Causse S., Bonan N. B., Dumétier B., Garrido C (2020) Heat-shock proteins: chaperoning DNA repair. *Oncogene* **39**:516-529 https://doi.org/10.1038/s41388-019-1016-y | PubMed
4. **Truman A. W.,** et al. (2012) CDK-Dependent Hsp70 Phosphorylation Controls G1 Cyclin Abundance and Cell-Cycle Progression. *Cell* **151**:1308-1318 https://doi.org/10.1016/j.cell.2012.10.051 | PubMed
5. **Chen Y.-J.,** et al. (2014) HSP70 colocalizes with PLK1 at the centrosome and disturbs spindle dynamics in cells arrested in mitosis by arsenic trioxide. *Arch. Toxicol* **88**:1711-1723 https://doi.org/10.1007/s00204-014-1222-x | PubMed
6. **Vergés E.,** Colomina N., Garí E., Gallego C., Aldea M (2007) Cyclin Cln3 Is Retained at the ER and Released by the J Chaperone Ydj1 in Late G1 to Trigger Cell Cycle Entry. *Mol. Cell* **26**:649-662 https://doi.org/10.1016/j.molcel.2007.04.023 | PubMed
7. **Evans C. G.,** Wisén S., Gestwicki J. E (2006) Heat Shock Proteins 70 and 90 Inhibit Early Stages of Amyloid β-(1–42) Aggregation in Vitro *. *J. Biol. Chem* **281**:33182-33191 https://doi.org/10.1074/jbc.m606192200 | PubMed
8. **Valle-Medina A.,** Calzada-Mendoza C. C., Ocharan-Hernández M. E., Jiménez-Zamarripa C. A., Juárez-Cedillo T (2025) Heat shock protein 70 in Alzheimer's disease and other dementias: A possible alternative therapeutic. *J. Alzheimer's Dis. Rep* **9** https://doi.org/10.1177/25424823241307021 | PubMed

9. **Calderwood S. K.,** Murshid A (2017) Molecular Chaperone Accumulation in Cancer and Decrease in Alzheimer's Disease: The Potential Roles of HSF1. *Front. Neurosci* **11** https://doi.org/10.3389/fnins.2017.00192 | PubMed

10. **Beltrao P.,** et al. (2012) Systematic Functional Prioritization of Protein Posttranslational Modifications. *Cell* **150**:413-425 https://doi.org/10.1016/j.cell.2012.05.036 | PubMed

11. **Preissler S.,** et al. (2015) AMPylation matches BiP activity to client protein load in the endoplasmic reticulum. *eLife* **4**:e12621 https://doi.org/10.7554/eLife.12621 | PubMed

12. **Preissler S.,** et al. (2017) AMPylation targets the rate-limiting step of BiP's ATPase cycle for its functional inactivation. *eLife* **6**:e29428 https://doi.org/10.7554/eLife.29428 | PubMed

13. **Moss S. M.,** et al. (2019) A Legionella pneumophila Kinase Phosphorylates the Hsp70 Chaperone Family to Inhibit Eukaryotic Protein Synthesis. *Cell Host Microbe* **25**:454-462.e6 https://doi.org/10.1016/j.chom.2019.01.006 | PubMed

14. **Albuquerque C. P.,** et al. (2008) A Multidimensional Chromatography Technology for In-depth Phosphoproteome Analysis. *Mol. Cell. Proteom* **7**:1389-1396 https://doi.org/10.1074/mcp.m700468-mcp200 | PubMed

15. **Holt L. J.,** et al. (2009) Global Analysis of Cdk1 Substrate Phosphorylation Sites Provides Insights into Evolution. *Science* **325**:1682-1686 https://doi.org/10.1126/science.1172867 | PubMed

16. **Russell R.,** Karzai A. W., Mehl A. F., McMacken R (1999) DnaJ Dramatically Stimulates ATP Hydrolysis by DnaK: Insight into Targeting of Hsp70 Proteins to Polypeptide Substrates †. *Biochemistry* **38**:4165-4176 https://doi.org/10.1021/bi9824036 | PubMed

17. **Preissler S.,** Rato C., Perera L. A., Saudek V., Ron D (2017) FICD acts bifunctionally to AMPylate and de-AMPylate the endoplasmic reticulum chaperone BiP. *Nat. Struct. Mol. Biol* **24**:23-29 https://doi.org/10.1038/nsmb.3337 | PubMed

18. **Rinaldi S.,** et al. (2018) A Local Allosteric Network in Heat Shock Protein 70 (Hsp70) Links Inhibitor Binding to Enzyme Activity and Distal Protein–Protein Interactions. *ACS Chem. Biol* **13**:3142-3152 https://doi.org/10.1021/acschembio.8b00712 | PubMed

19. **Buchberger A.,** et al. (1995) Nucleotide-induced Conformational Changes in the ATPase and Substrate Binding Domains of the DnaK Chaperone Provide Evidence for Interdomain Communication (*). *J. Biol. Chem* **270**:16903-16910 https://doi.org/10.1074/jbc.270.28.16903 | PubMed

20. **Kundel F.,** et al. (2018) Hsp70 Inhibits the Nucleation and Elongation of Tau and Sequesters Tau Aggregates with High Affinity. *ACS Chem. Biol* **13**:636-646 https://doi.org/10.1021/acschembio.7b01039 | PubMed

21. **Lee P.-C.,** Machner M. P (2018) The Legionella Effector Kinase LegK7 Hijacks the Host Hippo Pathway to Promote Infection. *Cell Host Microbe* **24**:429-438.e6 https://doi.org/10.1016/j.chom.2018.08.004 | PubMed

22. **Thomas E. N.,** Kim K. Q., McHugh E. P., Marcinkiewicz T., Zaher H. S (2020) Alkylative damage of mRNA leads to ribosome stalling and rescue by trans translation in bacteria. *eLife* **9**:e61984 https://doi.org/10.7554/eLife.61984 | PubMed

23. **Beard W. A.,** Horton J. K., Prasad R., Wilson S. H (2019) Eukaryotic Base Excision Repair: New Approaches Shine Light on Mechanism. *Annu. Rev. Biochem* **88**:137-162 https://doi.org/10.1146/annurev-biochem-013118-111315 | PubMed

24. **Sedgwick B.** (2004) Repairing DNA-methylation damage. *Nat. Rev. Mol. Cell Biol.* **5**:148-157 https://doi.org/10.1038/nrm1312 | PubMed

25. **Wyatt M. D.,** Pittman D. L (2006) Methylating Agents and DNA Repair Responses: Methylated Bases and Sources of Strand Breaks. *Chem. Res. Toxicol* **19**:1580-1594 https://doi.org/10.1021/tx060164e | PubMed

26. **Fu D.,** Calvo J. A., Samson L. D (2012) Balancing repair and tolerance of DNA damage caused by alkylating agents. *Nat. Rev. Cancer* **12**:104-120 https://doi.org/10.1038/nrc3185 | PubMed

27. **Sobol R. W.,** et al. (2003) Base Excision Repair Intermediates Induce p53-independent Cytotoxic and Genotoxic Responses*. *J. Biol. Chem* **278**:39951-39959 https://doi.org/10.1074/jbc.m306592200 | PubMed

28. **Srivastava D. K.,** et al. (1998) Mammalian abasic site base excision repair. Identification of the reaction sequence and rate-determining steps. *J. Biol. Chem* **273**:21203-21209 https://doi.org/10.1074/jbc.273.33.21203 | PubMed

29. **Horton J. K.,** Prasad R., Hou E., Wilson S. H (2000) Protection against Methylation-induced Cytotoxicity by DNA Polymerase β-Dependent Long Patch Base Excision Repair*. *J. Biol. Chem* **275**:2211-2218 https://doi.org/10.1074/jbc.275.3.2211 | PubMed

30. **Bau D.-T.,** et al. (2002) Oxidative DNA adducts and DNA-protein cross-links are the major DNA lesions induced by arsenite. *Environ. Heal. Perspect* **110**:753-756 https://doi.org/10.1289/ehp.02110s5753 | PubMed

31. **Ebert F.,** et al. (2011) Arsenicals affect base excision repair by several mechanisms. *Mutat. Res.Fundam. Mol. Mech. Mutagen* **715**:32-41 https://doi.org/10.1016/j.mrfmmm.2011.07.004 | PubMed

32. **Sykora P.,** Snow E. T (2008) Modulation of DNA polymerase beta-dependent base excision repair in cultured human cells after low dose exposure to arsenite. *Toxicol. Appl. Pharmacol* **228**:385-394 https://doi.org/10.1016/j.taap.2007.12.019 | PubMed

33. **Caldecott K. W** (2008) Single-strand break repair and genetic disease. *Nat. Rev. Genet* **9**:619-631 https://doi.org/10.1038/nrg2380 | PubMed

34. **Nikolova T.,** Ensminger M., Löbrich M., Kaina B (2010) Homologous recombination protects mammalian cells from replication-associated DNA double-strand breaks arising in response to methyl methanesulfonate. *DNA Repair* **9**:1050-1063 https://doi.org/10.1016/j.dnarep.2010.07.005 | PubMed

35. **Ensminger M.,** et al. (2014) DNA breaks and chromosomal aberrations arise when replication meets base excision repair. *J. Cell Biol* **206**:29-43 https://doi.org/10.1083/jcb.201312078 | PubMed

36. **Polyzos A. A.,** et al. (2024) Base excision repair and double strand break repair cooperate to modulate the formation of unrepaired double strand breaks in mouse brain. *Nat. Commun* **15**:7726 https://doi.org/10.1038/s41467-024-51906-5 | PubMed

37. **Giglia-Mari G.,** Zotter A., Vermeulen W. (2011) DNA Damage Response. *Cold Spring Harb. Perspect. Biol.* **3**:a000745 https://doi.org/10.1101/cshperspect.a000745 | PubMed

38. **Durocher D.,** Jackson S. P. DNA-PK (2001) ATM and ATR as sensors of DNA damage: variations on a theme?. *Curr. Opin. Cell Biol* **13**:225-231 https://doi.org/10.1016/s0955-0674(00)00201-5 | PubMed

39. **Lowndes N. F.,** Murguia J. R (2000) Sensing and responding to DNA damage. *Curr. Opin. Genet. Dev* **10**:17-25 https://doi.org/10.1016/s0959-437x(99)00050-7 | PubMed

40. **Caron P.,** et al. (2015) Non-redundant Functions of ATM and DNA-PKcs in Response to DNA Double-Strand Breaks. *Cell Rep* **13**:1598-1609 https://doi.org/10.1016/j.celrep.2015.10.024 | PubMed

41. **Heijink A. M.,** Krajewska M., Vugt M. A. T. M. van (2013) The DNA damage response during mitosis. *Mutat. Res.Fundam. Mol. Mech. Mutagen* **750**:45-55 https://doi.org/10.1016/j.mrfmmm.2013.07.003 | PubMed

42. **Lanz M. C.,** Dibitetto D., Smolka M. B (2019) DNA damage kinase signaling: checkpoint and repair at 30 years. *EMBO J* **38**:EMBJ2019101801 https://doi.org/10.15252/embj.2019101801 | PubMed

43. **Choi S.,** Gamper A. M., White J. S., Bakkenist C. J (2010) Inhibition of ATM kinase activity does not phenocopy ATM protein disruption. *Cell Cycle* **9**:4052-4057 https://doi.org/10.4161/cc.9.20.13471 | PubMed

44. **Menolfi D.,** Zha S. ATM (2020) ATR and DNA-PKcs kinases—the lessons from the mouse models: inhibition ≠ deletion. *Cell Biosci* **10** https://doi.org/10.1186/s13578-020-0376-x | PubMed

45. **Zannini L.,** Delia D., Buscemi G (2014) CHK2 kinase in the DNA damage response and beyond. *J. Mol. Cell Biol* **6**:442-457 https://doi.org/10.1093/jmcb/mju045 | PubMed

46. **Tuppi M.,** et al. (2018) Oocyte DNA damage quality control requires consecutive interplay of CHK2 and CK1 to activate p63. *Nat. Struct. Mol. Biol* **25**:261-269 https://doi.org/10.1038/s41594-018-0035-7 | PubMed

47. **Canman C. E.,** et al. (1998) Activation of the ATM Kinase by Ionizing Radiation and Phosphorylation of p53. *Science* **281**:1677-1679 https://doi.org/10.1126/science.281.5383.1677 | PubMed

48. **Chou W.-C.,** Hu L.-Y., Hsiung C.-N., Shen C.-Y (2015) Initiation of the ATM-Chk2 DNA damage response through the base excision repair pathway. *Carcinogenesis* **36**:832-840 https://doi.org/10.1093/carcin/bgv079 | PubMed

49. **Werner-Washburne M.,** Stone D. E., Craig E. A (1987) Complex Interactions Among Members of an Essential Subfamily of hsp70 Genes in Saccharomyces Cerevisiae. *Mol. Cell. Biol* **7**:2568-2577 https://doi.org/10.1128/mcb.7.7.2568-2577.1987 | PubMed

50. **Craig E. A.,** Jacobsen K (1984) Mutations of the heat inducible 70 kilodalton genes of yeast confer temperature sensitive growth. *Cell* **38**:841-849 https://doi.org/10.1016/0092-8674(84)90279-4 | PubMed

51. **Moreno D. F.,** et al. (2019) Proteostasis collapse, a hallmark of aging, hinders the chaperone-Start network and arrests cells in G1. *eLife* **8**:e48240 https://doi.org/10.7554/eLife.48240 | PubMed

52. **Caldecott K. W** (2020) Mammalian DNA base excision repair: Dancing in the moonlight. *DNA Repair* **93** https://doi.org/10.1016/j.dnarep.2020.102921 | PubMed

53. **Hantschel O** (2015) Unexpected Off-Targets and Paradoxical Pathway Activation by Kinase Inhibitors. *ACS Chem. Biol* **10**:234-245 https://doi.org/10.1021/cb500886n | PubMed

54. **Jackson A. L.,** Linsley P. S (2010) Recognizing and avoiding siRNA off-target effects for target identification and therapeutic application. *Nat. Rev. Drug Discov* **9**:57-67 https://doi.org/10.1038/nrd3010 | PubMed

55. **Blackford A. N.,** Stucki M (2020) How Cells Respond to DNA Breaks in Mitosis. *Trends Biochem. Sci* **45**:321-331 https://doi.org/10.1016/j.tibs.2019.12.010 | PubMed

56. **Pramanik S.,** Chen Y., Bhakat K. K. (2024) Base Excision Repair in Mitotic Cells and the Role of Apurinic/Apyrimidinic Endonuclease 1 (APE1) in Post-Mitotic Transcriptional Reactivation of Genes. *Int. J. Mol. Sci.* **25**:12735 https://doi.org/10.3390/ijms252312735 | PubMed

57. **Fontaine S. N.,** et al. (2015) Isoform-selective Genetic Inhibition of Constitutive Cytosolic Hsp70 Activity Promotes Client Tau Degradation Using an Altered Co-chaperone Complement*. *J. Biol. Chem* **290**:13115-13127 https://doi.org/10.1074/jbc.m115.637595 | PubMed

58. **Muller P.,** et al. (2013) C-terminal phosphorylation of Hsp70 and Hsp90 regulates alternate binding to co-chaperones CHIP and HOP to determine cellular protein folding/degradation balances. *Oncogene* **32**:3101-3110 https://doi.org/10.1038/onc.2012.314 | PubMed

59. **Nitika,** Truman A. W. (2017) Cracking the Chaperone Code: Cellular Roles for Hsp70 Phosphorylation. *Trends Biochem. Sci* **42**:932-935 https://doi.org/10.1016/j.tibs.2017.10.002 | PubMed

60. **Pettersen E. F.,** et al. (2004) UCSF Chimera—A visualization system for exploratory research and analysis. *J. Comput. Chem* **25**:1605-1612 https://doi.org/10.1002/jcc.20084 | PubMed

61. **Chang L.,** Thompson A. D., Ung P., Carlson H. A., Gestwicki J. E (2010) Mutagenesis Reveals the Complex Relationships between ATPase Rate and the Chaperone Activities of Escherichia coli Heat Shock Protein 70 (Hsp70/DnaK)*. *J. Biol. Chem* **285**:21282-21291 https://doi.org/10.1074/jbc.m110.124149 | PubMed

62. **Chang L.,** et al. (2008) High-throughput screen for small molecules that modulate the ATPase activity of the molecular chaperone DnaK. *Anal. Biochem* **372**:167-176 https://doi.org/10.1016/j.ab.2007.08.020 | PubMed

63. **Nadel C. M.,** et al. (2024) Phosphorylation of tau at a single residue inhibits binding to the E3 ubiquitin ligase, CHIP. *Nat. Commun* **15**:7972 https://doi.org/10.1038/s41467-024-52075-1 | PubMed

64. **Zhang H.,** Siede W (2003) Analysis of the Budding Yeast Saccharomyces cerevisiae Cell Cycle by Morphological Criteria and Flow Cytometry. In: Lieberman H. B. (Ed). *Cell Cycle Checkpoint Control Protocols* Springer Nature. pp. 77-91

65. **Rosebrock A. P** (2017) Analysis of the Budding Yeast Cell Cycle by Flow Cytometry. *Cold Spring Harb. Protoc* https://doi.org/10.1101/pdb.prot088740 | PubMed

66. **Omkar S.,** et al. (2025) Mechanosensor-mediated Hsp70 phosphorylation orchestrates the landscape of the heat shock response. *Nat. Commun* **17** https://doi.org/10.1038/s41467-025-67204-7 | PubMed

67. **Backe S. J.,** Heritz J. A., Mollapour M (2025) Hsp70 and Hsp90 post-translational modifications and translating the chaperone code. *Cell Stress Chaperones* **30** https://doi.org/10.1016/j.cstres.2025.100118 | PubMed

Peer reviews

Reviewer #1 (Public review):

Summary:

This study identifies a conserved phosphorylation event on Hsp70, at human T495 that is triggered by DNA damage. The authors show that this modification arises in response to MMS and is temporally associated with cell cycle progression through mitosis. Using biochemical analysis, they further argue that the phosphomimetic Hsc70(T495E) adopts an open-like conformation with impaired J protein-stimulated ATP hydrolysis while still retaining client binding. In yeast, both phosphomimetic and phosphonull mutants perturb growth and cell cycle progression, supporting the idea that dynamic regulation of this site helps coordinate DNA damage responses with G1/S control.

Strengths:

A major strength of the paper is that it links prior work on Legionella-mediated Hsp70 phosphorylation to a normal cellular DNA damage response. The study is also commendably multi-level, combining mammalian cell biology, in vitro biochemistry, and yeast genetics to support the central model. Together, the authors provide a coherent story that this Hsp70 site has functional importance in checkpoint-like control rather than being a passive phosphosite, adding to our understanding of the chaperone code.

Minor Weaknesses:

The authors acknowledge that the direct kinases/phosphatases for this site remain unknown. Some conclusions are therefore still somewhat inferential, especially the model that pHsp70 acts as a reversible molecular brake on S-phase entry. These limitations do not undermine the importance of these exciting findings, but they do leave the paper somewhat short of a fully resolved mechanism.

Comments on revisions:

The authors have done a great job in addressing all the previous reviewer concerns. They have provided additional data and refined the text, stating limitations of their proposed model. In doing so, they have produced a much-improved version of the manuscript.

https://doi.org/10.7554/eLife.110044.2.sa3

Reviewer #2 (Public review):

The revised manuscript offers little new information and fails to address the critical weaknesses identified in the original submission.

While we can agree that phosphorylation of Thr495 would likely affect Hsp70 function-given the known biochemistry of Hsp70s and the author's previous work on LegK4-the significance of this finding hinges on whether it is a regulated process. If a meaningful fraction of Hsp70 were phosphorylated in a regulated manner triggered by DNA damage or cell cycle progression, it would constitute an important discovery, regardless of its specific impact on fitness in a given context.

However, beyond highlighting the temporal profile of Hsp70 phosphorylation in MMS-treated cells (Figure 4e), the paper fails to rule out the possibility that this correlation is merely an irrelevant side reaction. This "bystander" phosphorylation could simply be caused by the activation of kinases during the experimental MMS treatment and subsequent washout. The authors' claim-that the fraction of phosphorylated Hsp70 increases in a "regulated, cell-cycle dependent manner"-does not sufficiently counter the possibility of it being a non-functional side effect.

This concern could be resolved if the authors had identified the specific kinase, demonstrated its specificity, and manipulated it either genetically or pharmacologically. While I acknowledge this is a "tall order," the lack of such data limits the paper's significance. Furthermore, the current data fails to meet a much lower bar: confirming that a substantial fraction of Hsp70 is actually phosphorylated under the tested conditions. Such a finding would at least suggest the event is capable of impacting the overall Hsp70 pool.

It is surprising that the authors have not provided a ratiometric assay to settle this, such as an immunoblot of total Hsp70 separated on a Phos-tag or IEF gel. Instead, they rely on indirect evidence and data subject to alternative interpretations. Specifically, they argue that the fitness cost of the Thr495Ala mutation (or the phosphomimetic mutation) is due to the loss of regulatory phosphorylation (or deregulated phosphorylation); however, it is equally plausible that the mutations create Hsp70 hypomorphs whose defects are only exposed under stressful experimental conditions.

https://doi.org/10.7554/eLife.110044.2.sa2

Reviewer #3 (Public review):

In this manuscript Moss et al. demonstrate that Hsp70 phosphorylation at a conserved threonine residue integrates DNA damage responses with cell-cycle control. The authors present unbiased biochemical, cell-based, and yeast genetic analyses showing that phosphorylation of human Hsp70 at T495 (and the analogous Ssa1 T492 in yeast) is triggered by base-excision-repair intermediates and downstream DDR kinase activity, leading to delayed G1/S progression after DNA damage. They used orthogonal approaches such as ATPase assays, phospho-specific detection, kinase-inhibition studies, synchronization experiments, and phenotypic analyses of phosphomutants. They presented robust data which collectively supported the conclusion that dynamic Hsp70 phosphorylation functions as a conserved "molecular brake" to prevent inappropriate S-phase entry under genotoxic stress.

Comments on revisions:

The authors have addressed all my questions and concerns.

https://doi.org/10.7554/eLife.110044.2.sa1

Author response:

The following is the authors' response to the original reviews

We thank the reviewers for their time and consideration of the manuscript. We have added new data to Figure 5 (Figure 5a) to address concerns regarding the conservation of the Hsp70 phosphorylation in yeast. Additionally, we have changed the title of the manuscript to “Hsp70 is phosphorylated in a conserved response to DNA damage and contributes to cell cycle control” to more accurately represent the conclusions we draw.

> ***Public Reviews:***
>
> ***Reviewer #1 (Public review):***
>
> *The strength of evidence of the mechanistic and "conserved checkpoint" claims that this site is directly activated by DNA damage is inadequate and fundamentally incorrect.*

We respectfully disagree with the reviewer’s characterization of our conclusions. Our data demonstrate that DNA damage induces this phosphorylation in a cell-cycle–dependent manner. We do not claim to have defined the direct kinase or full mechanistic pathway; rather, we establish that site activation is damage-responsive and functionally linked to cell-cycle regulation. Consistent with this, phospho-mutants in yeast exhibit clear cell-cycle defects, supporting a conserved functional role. We address each of the reviewer’s specific concerns below.

> *Specific comments:*
>
> *(1) Activation of T495:*
>
> *The author's premise for the site being activated by DNA damage is Albuquerque et al, where PTMs on MMS treated yeast are analyzed. T492 (the yeast equivalent of human T495) is observed as phosphorylated. However, the authors fail to note that there is no untreated sample analysis in this study, and it is likely that T492 phosphorylation is also present in untreated cells. This is also backed up by later evidence from the same lab (Smolka et al), where they do not identify T492 as being dependent on Mec1/Tel/Rad53 kinases.*

We agree with this assessment of the Albuquerque study. Accordingly, we used their data to generate the hypothesis that this site is phosphorylated, and we took it upon ourselves to more rigorously demonstrate phosphorylation with appropriate controls. The validated antibody that we had previously generated[1] to track pHsp70 was the enabling technology to directly track this phosphorylation event. We now directly show phosphorylation of this site (Figure 5a, lines 276-284). Of note, as Reviewer 1 suggested, there is a smaller amount of pHsp70 in the untreated cells, which corresponds with findings from Holt et al 2009 [2]. This could reflect a baseline role of Hsp70 phosphorylation for normal growth that is accentuated upon MMS insult.

> *(2) The kinase(s) directly responsible for T495 phosphorylation are not identified. Instead, the authors show that knockdown or pharmacological inhibition of DNA-PKcs, ATM, Chk2, and CK1 attenuate pHsp70.*

We agree with reviewer 1 that identifying the direct kinase would be an exciting finding, and we believe our manuscript will provide the foundation for future studies to address these questions. While these findings will be impactful, we do not believe their lack detracts from the observations we have made.

> *(3) ATM siRNA knockdown has no effect, while ATM inhibitors do, which the authors acknowledge but do not resolve. This discrepancy raises concerns about off-target drug effects.*

We agree with reviewer 1 that off-target drug effects are always a concern when employing pharmacological inhibitors. To that end, we tested structurally distinct inhibitors of ATM (Figure 3b) to decrease the likelihood of the same off target effect. While complementing this with a genetic knockdown would be ideal, the discrepancies between pharmacological and genetic inhibition of ATM have been well reported (lines 214-216).[3,4] Parallel discrepancies in other kinases have been mechanistically explored by other groups.[5] The preponderance of pharmacological evidence in conjunction with RNAi suggests the most likely interpretation of our data is that ATM is involved in signaling upstream of Hsp70 phosphorylation. Thus, our data compel future work to use more sophisticated genetic methods to more specifically determine how ATM connects with pHsc70.

> *(4) No in vitro kinase assays, motif analysis, or phosphosite mapping confirming these kinases as direct T495 kinases are presented. Thus, the proposed signaling cascade remains speculative.*

We agree that we should carefully circumscribe our conclusions about the potential signaling cascade. To communicate our conclusions more clearly, we rewrote lines 223-226 to highlight that our findings implicate these kinases in upstream signaling rather than direct phosphorylation of Hsp70.

> *(5) Smolka and many other labs characterized DDR sites as SQ/TQ motifs, and T492 doesn't fit that motif.*

We agree, and our response to comment 4 addresses this point. Briefly, we do not claim that Hsp70 is a direct target for DDR. Notably, the SQ/TQ motifs mentioned specifically pertain to ATM and DNA-PK[6], though we would like to note several studies have demonstrated DNA-PK phosphorylation outside of these motifs.[7] Chk2 and CK1 do not prefer SQ/TQ motifs[9]. Additionally, Chk2 is known to phosphorylate non-consensus sequences as well[10].

> *(6) No genetic tests in yeast (e.g., BER mutants) are used to connect Ssa1 T492 phosphorylation to BER in that system, despite the strong BER-centric model.*

We agree that it would be interesting to study BER mutants in yeast, and we believe this will be an exciting prospect for future studies to better establish the signaling cascade. We have included a Western blot (Figure 5a) showing that MMS treatment causes increased Hsp70 phosphorylation in yeast. MMS damage is repaired through BER in *S. cerevisiae*,[11] and the pathway itself is highly conserved.[12] Our experiments demonstrate that the phosphorylation of Hsp70 occurs as a conserved response to alkylation damage, which is the major conclusion of our paper.

> *(7) Overexpression of MPG gives only a modest increase in pHsp70, while APE1 overexpression has no effect, and Polβ overexpression does not decrease pHsp70. These mixed results weaken the central claim that Hsp70 phosphorylation is a tuned sensor of BER burden.*

We appreciate this incisive question. Though not immediately intuitive, we do not believe these results are necessarily 'mixed'. The lack of APE1 over-expression having an effect could be attributed to APE1 activity being necessary for the phosphorylation, but not rate-limiting. Regarding Polβ, it is important to note that not its binding, but rather its dRP lyase activity is rate-limiting in base excision repair.[13] As such, if binding sites are already saturated or near saturated, but the lyase activity remains slow, we may not observe a decrease in BER intermediates. While we do claim that phosphorylation of Hsp70 is triggered by BER intermediates (lines 193-194), we do not claim that pHsp70 is a tuned sensor of BER burden.

> *(8) A major concern is that pHsp70 is only convincingly detected after very high, prolonged MMS (10 mM, 5 h) or 0.5 mM arsenite treatments. Other DNA-damaging*

> *agents (bleomycin, camptothecin, hydroxyurea) that robustly activate DDR kinases do not induce pHsp70. This suggests to me that the authors are observing a side effect of proteotoxic stress. This is likely (see Paull et al, PMID: 34116476).*

Our data indicate that pHsp70 specifically occurs downstream of base excision repair. Therefore, it is not surprising that drugs that do not activate BER (bleomycin, camptothecin, hydroxyurea) do not elicit the same response. While pHsp70 may arise due to DSBs generated through BER, the fact we do not see phosphorylation after bleomycin treatment could be explained by the cell-cycle dependencies we report (Figure 4e). It is also important to note that MMS-induced pHsp70 occurs primarily in the nucleus, and Western blots of whole cell lysate will contain large amounts of cytosolic Hsp70 that could dilute the signal. Indeed, in our nuclear extraction (Figure 4d), we see faint pHsp70 signal as soon as 1 h after treatment, though it increases in robustness as the time-course progresses. These data are both concordant with a model in which high BER-induced lesion burden in mitosis leads to Hsp70 phosphorylation in late M/G1.

We would like to add that, in the review article cited by Reviewer 1, the authors specifically cite studies implicating a loss-of-function in DDR pathways leading to increased proteotoxic stress (e.g. ATM deficient cells producing higher levels of aggregated proteins compared to WT). However, we find that inhibition of DDR kinases decreases, rather than increases Hsp70 phosphorylation. We thus believe that DNA damage rather than proteotoxic stress is the parsimonious cause of Hsp70 phosphorylation.

> *(9) A recent study in Nature Communications (Omkar et al., 2025) demonstrates rapid phosphorylation of yeast T492 in a pkc1-dependent manner, diminishing the impact of these findings.*

We were excited to see this paper when it was published 3 months after we posted a preprint on bioRxiv, which was released three weeks after our submission to eLife. Rather than diminishing the impact of this paper, we believe that independent lines of evidence from different groups mutually reinforces the impact of the work. We have added a sentence to say that during the review of our work, this group independently observed this phosphorylation event in response to a different stress (lines 421-423). We believe in celebrating the scientific process arriving at consistent results, and the editorial policies of eLife reinforce that philosophy by offering ‘scoop protection.’

We would also like to highlight several differences between the scope of our papers. The phosphorylation reported by Omkar et al. appears highly constrained to yeast as part of the Cell Wall Integrity pathway, whereas ours occurs as a more highly conserved response. Additionally, our paper provides additional biochemical insight into the consequences of this phosphorylation, which is lacking in Omkar et al. If anything, this paper highlights the important regulatory capacity of this residue on Hsp70, and suggests it may serve multiple functions in the cell.

> *(2) Downstream Effects of T492/T495:*
>
> *(10) The manuscript's central conceptual advance is that pHsp70 is a cell-cycle-regulated brake on G1/S. Yet in mammalian cells, the authors show only that pHsp70 appears late, after cells have traversed mitosis, and that blocking CDK1 (G2/M) prevents its accumulation.*

We would like to clarify the central contribution of this study. Prior work identified this phosphorylation in yeast, but its existence and conservation in human cells had not been established. A primary advance of our study is demonstrating that this site is phosphorylated in mammalian cells and that its accumulation is cell-cycle regulated — coinciding with late M/G1.

We further show that phosphorylation depends on cell-cycle progression, as CDK1 inhibition prevents its accumulation. While these data establish regulation, we agree that they do not by themselves define causality in mammalian cells. To address functional consequences, we leveraged the genetic tractability of *S. cerevisiae*. Phosphomimetic Ssa1 T492E increases the proportion of G1 cells in the absence of MMS and enforces a stronger G1 arrest following MMS treatment. Together, these findings support a conserved, cell-cycle–linked role for this phosphorylation and provide a foundation for future mechanistic work in mammalian systems.

> *(11) There is no functional test in human cells: no knockdown/rescue experiments with T495A or T495E, no cell-cycle profiling upon altering Hsp70 phosphorylation state, and no demonstration that pHsp70 actually causes any delay in S-phase entry, rather than simply correlating with late damage responses. The strong conclusion that pT495 "stalls cell cycle progression" (e.g., Figure 6 model) is therefore not supported in the human system.*

We agree that we did not directly test the functional consequences of Hsp70 phosphorylation in human cells. Our intent was not to claim that we have demonstrated causality in the mammalian system, but rather to establish that this conserved phosphorylation exists in human cells and is cell-cycle regulated.

We instead used *S. cerevisiae* to interrogate this due to its increased genetic tractability. In this system, phosphomimetic mutation increases the proportion of G1 cells under basal conditions and enhances G1 arrest following MMS treatment, mirroring the damage-associated phenotype observed in human cells. These findings support a conserved functional role for this modification, although we agree that direct mechanistic testing in mammalian cells will be important for future work.

While we intended the cartoon model to be a speculative illustration of what may be occurring in order to motivate future studies. We now see how this may lead to confusion, so to improve clarity, we have removed Figure 6 from the manuscript.

> *(12) All functional conclusions rely on T492A/E point mutants at the endogenous SSA1 locus, usually in an ssa2Δ background, in a family of highly redundant Hsp70s. Without showing that this site is actually modified during their MMS treatments, the assignment of phenotypes to loss of a physiological phospho-switch is premature. The authors need to repeat their studies in an Ssa1-4 background, as in https://pubmed.ncbi.nlm.nih.gov/32205407/.*

Thank you for this feedback. We have included a Western blot to Figure 5 (Figure 5a) addressing this comment. Briefly, we show that, in yeast, Hsp70 phosphorylation increases upon MMS treatment and is not detectable in the point-mutants in the *ssa2Δ* background. The latter data suggest that Ssa3-4 modification is negligible in our system.

> *(13) The authors infer that T495E "locks" Hsc70 in a pseudo-open state based on reduced J-protein-stimulated ATPase activity, unchanged ATP binding, altered trypsin sensitivity, and retained tau binding. However, there is no direct comparison of phosphorylated vs T495E protein (e.g., via in vitro phosphorylation with LegK4 followed by side-by-side biochemical assays, or structural analysis). Thus, it remains unclear to what extent the glutamate substitution mimics a phosphate at this position.*

Previously we did show that phosphorylation impacts the ATPase cycle of Hsp70.[1] In this paper, with the phosphomimetic mutant we see an even greater decrease of activity. This is consistent with incomplete phosphorylation yielded by *in vitro* phosphorylation with LegK4. [1] Due to this incomplete phosphorylation *in vitro*, we determined that the phosphomimetic mutant would be more useful for the assays we performed, as they rely on bulk readouts.

> *(14) No client release kinetics, co-chaperone binding assays, or in vivo chaperone function tests are provided, yet the discussion builds a detailed model of a "pseudo-open" state that simultaneously resembles ATP-bound conformation and allows persistent substrate engagement.*

We have shown that the conformational cycle of Hsp70 (T495E) is uncoupled from nucleotide state, and that the overall conformation resembles ATP-bound Hsp70. This is consistent with prior studies on AMPylation of the same residue.[14] Additionally, we demonstrate that substrate engagement is similar between WT and T495E. This is consistent with our previously published work showing increased pHsp70 on polysomes,[1] as well as our observations that the phosphomimetic mutant in yeast exerts a phenotype even in the presence of the compensatory isoform SSA2. This dominant-like phenotype is consistent with those seen in mutations locking Hsp70 in a 'closed' conformation.[15] We agree that future studies examining client release kinetics and co-chaperone binding would be useful for future structural studies validating and elaborating on our findings.

> ***Reviewer #2 (Public review):***
>
> *Weaknesses:*
>
> *The kinase(s) responsible for the phosphorylation have not been identified (and hence remain inaccessible to experimental i.e., genetic or pharmacological manipulation). The mechanistic links to DNA damage repair and the fitness benefits of this proposed adaptation remain obscure. Of greater concern, the data provided in the paper fail to exclude the trivial possibility that the phosphorylation event described (and characterized through biochemical proxies) is biologically neutral, reflecting nothing more than a bystander event in which kinase(s) activated by application of high concentrations of a powerful alkylating agent (MMS) phosphorylate, at meaninglessly low stoichiometry, an abundant protein (Hsp70) on a surface exposed residue. Failure to exclude this (plausible) scenario is this paper's weakness.*

We agree that we have not directly quantified the absolute stoichiometry of Hsp70 phosphorylation. However, several lines of evidence argue against the interpretation that this represents a biologically neutral, bystander modification.

First, our pulse-chase experiment (Figure 4e) shows that, after MMS removal, pHsp70 levels increase as cells progress through the cell cycle. Notably, total Hsp70 levels remain constant. This indicates that the fraction of phosphorylated Hsp70 increases in a regulated, cell-cycle dependent manner, rather than through a bystander event during acute stress.

Second, functional perturbation of the homologous site in yeast produces phenotypic consequences. The phosphomimetic Ssa1(T492E) mutant exhibits reduced growth, increased G1 accumulation, and impaired cell-cycle re-entry following MMS treatment (Figure 5). These phenotypes argue that the modification of this residue is functionally consequential.

While the upstream kinase remains to be identified, the genetic and cell-cycle phenotypes observed upon site perturbation argue that this phosphorylation is functionally consequential.

> ***Reviewer #2 (Recommendations for the authors):***
>
> *(1) The biochemical characterization of the phosphomimetic mutation (T495E) is thorough, relying on ATPase assays and conformational analysis. Figure 1b demonstrates reduced J-protein-stimulated ATPase activity, and Figure 1d shows an ATP-like proteolysis pattern consistent with an open conformation. As the authors are well aware, Hsp70 chaperones act on their substrates via a dynamic cycle that includes*

> *binding, ATP hydrolysis, and conformational shifts. One wonders, therefore, at the relevance of the measurement shown in Figure 1f. While it is highly plausible that the T495E mutation mimics the phosphorylation event (BiP T518E mimics key aspects of AMPylation), the lack of a biochemical characterisation of Hsp70 with pThr495 is an important limitation of this paper. Even if such a preparation cannot be accomplished with the endogenous kinase(s) whose identity remains unknown, a characterisation of LegK4-phosphorylated Hsp70 should suffice.*

We agree with Reviewer 2 that the rationale for figure 1f does not logically follow the results of 1b and 1d. Rather, this experiment was motivated by the prior findings that phosphorylation of Hsp70 by *L.p.* lead to an increase occupancy on polysomes[1] (lines 137-139). We sought to better understand the discrepancy between this finding and our own by assaying the capacity of the T495E mutant to bind substrate.

Reviewer 2 raises a valid point in that phosphomimetic proteins do not necessarily behave the same as truly phosphorylated proteins. Previous work from our lab characterized the ATPase activity and *in vitro* folding capacity of Hsc70 that had been directly phosphorylated by LegK4[1] (lines 114-115). We were motivated to turn to a phosphomimetic mutant as LegK4 only phosphorylates around half of the Hsc70 present in solution[1] (line 116); this mixture of species makes batch analysis difficult. As we had previously published with the *in vitro* phosphorylated Hsc70, we didn't believe it necessary to include along with our future analyses.

> *(2) As noted, the kinase(s) that phosphorylate T495 remain to be identified and is inaccessible genetically. The phenotypic consequences of impaired pThr495 are therefore assessed by a T495A mutation. This most certainly eliminates phosphorylation at that site however, Figure 5C shows quite clearly that the T/A mutation is not neutral. This is expected, given the role of an H-bond network centered upon the homologous residue in the ADP-bound configuration of Hsp70's. Importantly, the biochemical non-neutrality of the T/A mutation also compromises the interpretation of the associated phenotype, as this cannot be attributed solely to a loss of phosphorylation; it may reflect features of the T/A mutations exposed by MMS, but unrelated to the inability of the residue to undergo regulated phosphorylation.*

We appreciate this insightful critique. We agree that the alanine substitution may perturb the local H-bond network, and have added a sentence to our discussion to highlight this caveat (lines 379-381). That being said, our conclusions do not solely rely on the T to A mutant. The phenotypes observed in our phosphomimetic mutant overlap with the TA mutant (increased sensitivity to MMS; defects in cell cycle re-entry after MMS treatment) (Figure 5). While the alanine mutation may not represent a purely 'loss-of-phosphorylation' state, our findings do implicate the importance of this residue in cell cycle control after DNA damage.

> *(3) It thus remains formally possible that pThr495 arises as an irrelevant side reaction due to activation of a kinase (with other relevant substrates).*
>
> *This dismal interpretation of the data would be dispelled somewhat if the stoichiometry of pThr495 were substantial, whereas very low stoichiometry of phosphorylation should leave one wary of the possibility that the surface-exposed Thr495 of ATP-bound Hsc70 is a physiologically irrelevant bystander target of a kinase activated in DNA-damaged cells.*

We have included a Western blot in Figure 5 showing pHsp70 in our yeast samples. Here we can see low abundance of Hsp70 phosphorylation in untreated WT yeast, with a clear increase in MMS treated yeast. Additionally, as mentioned in a previous response, Figure 4e shows the accumulation of pHsp70 in human cells even after MMS removal, indicating it is not simply the byproduct of over-activation of the DNA damage response.

> *Unfortunately, the study does not quantify the stoichiometry of Hsp70 phosphorylation; detection relies on phospho-specific immunoblotting, leaving open the question of whether this modification occurs at physiologically significant levels. This worry is compounded by Figure 2a,f that suggests that phosphorylation occurs only under high-dose MMS or arsenite, raising concerns about physiological relevance.*

We agree that we did not quantify absolute phosphorylation stoichiometry. While a precise measurement would be informative, our conclusions are based on regulated dynamics and functional perturbations rather than magnitude alone. Specifically, our pulse-chase (Figure 4e) shows that total Hsp70 levels remain constant while pHsp70 increases in a cell-cycle dependent manner following MMS removal. This indicates a regulated modification rather than a side-effect of kinase over-activation during acute stress. Additionally, perturbation of the homologous site produces cell-cycle phenotypes (Figure 5) in yeast, supporting functional relevance.

However, as mentioned in responses to Comment 3, our pulse-chase assay in Figure 4e indicates the stoichiometry of pHsp70 increases after MMS removal in a cell-cycle dependent manner. Furthermore, as discussed in response to Reviewer 1 Comment 8, Figure 4d highlights a technical limitation with regards to detection of pHsp70 by Western blotting. Namely, as pHsp70 accumulates in the nucleus, signal appears to be diluted by unmodified Hsp70 in the cytosol when whole-cell lysate is probed, thereby reducing detection capacity. It is therefore possible that less stringent doses do lead to phosphorylation, but due to the experiments being run in asynchronous cells and on whole cell lysate we failed to detect it.

> ***Reviewer #3 (Recommendations for the authors):***
>
> *Major Comments:*
>
> *(1) Figure 1e - Which antibody was used to probe this blot?*

Thank you for catching this omission. This was stained with Coomassie. We have edited the figure legend to reflect this.

> *(2) Figure 1c- Do the authors have the data of the WT and T495E with DJA2?*

The assay was performed with increasing concentrations of DJA2 for both constructs (from 0 μM to 4 μM) (lines 118-119, Figure 1c).

> *(3) Figure 2- The labeling of the right side of the immunoblots is missing.*

We apologize for the confusion. The labeling is on the left. The lines on the right are intended to demarcate blots that came from the same membrane (for easier comparison of loading controls).

> *(4) Figure 2d- Does MMS treatment lead to a heat shock response?*

We have not directly tested this. However, we do not see the massive upregulation of HSPs that would be expected from a heat shock response.

> *(5) Figure 4c and e - Total protein level of some of the phospho-proteins is missing.*

We used housekeeping proteins as loading control. We do not have antibodies for all the non-phospho proteins. For those we have, blots not included in the publication do not show any marked discrepancies between the non-phospho form and the housekeeping proteins.

> *(6) Figure S1A- Although the authors suggest that the phosphorylation event is reversible, they have not integrated it into the final model in Figure 6.*

In line 403 we postulate that dephosphorylation may permit client release. In the interest of clarity, we have now removed the model figure.

> *(7) Yeast genotype is missing.*

We used W303a yeast (line 612).

> *(8) It is unclear which phosphatase inhibitor was used in their assay (Figure S1A).*

We repeated the experiment with both Halt Phosphatase Inhibitor Cocktail (Thermo Scientific 78440) and Roche PhosStop (Roche 04906837001) (lines 524-525).

> *(9) Please add this most recent and up-to-date reference (PMID: 40976416) related to your study.*

We have now added that reference

> *(10) Can the authors speculate on whether Hsp70- T495E is expected to primarily reside in the nucleus?*

We have no data to indicate whether or not phosphorylation at T495 or a phosphomimetic mutation in this site would directly affect nuclear import or export. In cells expressing the *Legionella* kinase LegK4, pHsp70 exists in the cytoplasm,[1] indicating the phosphorylation in of itself does not force nuclear localization. We thus imagine that the nuclear localization seen in Figure 4d is more likely due to the location of the kinase rather than as a consequence of the phosphorylation. In an over-expression system or in the case of a genomic mutation, we believe the protein is most likely to exist in both the cytoplasm and in the nucleus, though we did not directly test this.

References

(1) Moss, S. M. et al. A Legionella pneumophila Kinase Phosphorylates the Hsp70 Chaperone Family to Inhibit Eukaryotic Protein Synthesis. Cell Host Microbe 25, 454-462.e6 (2019).

(2) Holt, L. J. et al. Global Analysis of Cdk1 Substrate Phosphorylation Sites Provides Insights into Evolution. Science 325, 1682–1686 (2009).

(3) Choi, S., Gamper, A. M., White, J. S. & Bakkenist, C. J. Inhibition of ATM kinase activity does not phenocopy ATM protein disruption. Cell Cycle 9, 4052–4057 (2010).

(4) Menolfi, D. & Zha, S. ATM, ATR and DNA-PKcs kinases—the lessons from the mouse models: inhibition ≠ deletion. Cell Biosci. 10, 8 (2020).

(5) Weiss, W. A., Taylor, S. S. & Shokat, K. M. Recognizing and exploiting differences between RNAi and small-molecule inhibitors. Nat. Chem. Biol. 3, 739–744 (2007).

(6) Kim, S.-T., Lim, D.-S., Canman, C. E. & Kastan, M. B. Substrate Specificities and Identification of Putative Substrates of ATM Kinase Family Members*. J. Biol. Chem. 274, 37538–37543 (1999).

(7) Jette, N. & Lees-Miller, S. P. The DNA-dependent protein kinase: A multifunctional protein kinase with roles in DNA double strand break repair and mitosis. Prog. Biophys. Mol. Biol. 117, 194–205 (2015).

(8) O'Neill, T. et al. Determination of Substrate Motifs for Human Chk1 and hCds1/Chk2 by the Oriented Peptide Library Approach*. J. Biol. Chem. 277, 16102–16115 (2002).

(9) Fulcher, L. J. & Sapkota, G. P. Functions and regulation of the serine/threonine protein kinase CK1 family: moving beyond promiscuity. Biochem. J. 477, 4603–4621 (2020).

(10) Craig, A. et al. Allosteric effects mediate CHK2 phosphorylation of the p53 transactivation domain. EMBO Rep. 4, 787–792 (2003).

(11) Xiao, W., Chow, B. L. & Rathgeber, L. The repair of DNA methylation damage in Saccharomyces cerevisiae. Curr. Genet. 30, 461–468 (1996).

(12) Memisoglu, A. & Samson, L. Base excision repair in yeast and mammals. Mutat. Res.Fundam. Mol. Mech. Mutagen. 451, 39–51 (2000).

(13) Srivastava, D. K. et al. Mammalian Abasic Site Base Excision Repair IDENTIFICATION OF THE REACTION SEQUENCE AND RATE-DETERMINING STEPS*. J. Biol. Chem. 273, 21203–21209 (1998).

(14) Preissler, S., Rato, C., Perera, L. A., Saudek, V. & Ron, D. FICD acts bifunctionally to AMPylate and de-AMPylate the endoplasmic reticulum chaperone BiP. Nat. Struct. Mol. Biol. 24, 23–29 (2017).

(15) Fontaine, S. N. et al. Isoform-selective Genetic Inhibition of Constitutive Cytosolic Hsp70 Activity Promotes Client Tau Degradation Using an Altered Co-chaperone Complement*. J. Biol. Chem. 290, 13115–13127 (2015).

https://doi.org/10.7554/eLife.110044.2.sa0